Proximity effect in superconductor-insulator-superconductor Josephson tunnel junctions: Theory and experiment

A. A. Golubov,* E. P. Houwman,† J. G. Gijsbertsen, V. M. Krasnov,* J. Flokstra, and H. Rogalla
University of Twente, Department of Applied Physics, P.O.B. 217, 7500 AE Enschede, The Netherlands

M. Yu. Kupriyanov
Nuclear Physics Research Institute, 119889 GSP Moscow, Russia
(Received 10 June 1994)

A microscopic model of the proximity effect in superconductor-insulator-superconductor ($SS'IS''S$) Josephson tunnel junctions has been developed for the general case of the finite critical temperature of the S' (S'') metal, arbitrary SS' (SS'') boundary transparency and the strength of the proximity effect between S and S' (respectively S and S''). The metals are assumed to be in the dirty limit and the thickness of the proximity layer is assumed to be small compared to its coherence length. The electrical properties of the $SS'IS''S$ junction are calculated as a function of the strength of the proximity effect, boundary transparency, critical temperature ratio, and temperature. The experimentally determined electrical characteristics of a series of Nb/Al_1, Al oxide, Al_2/Nb junctions with varying thickness d_1 of the Al_1 layer were interpreted with this model. The current-voltage characteristics and the temperature dependence of the critical current and sum-gap voltage could be described quantitatively well without any other correction than the non-BCS ratio $\Delta_0/k_BT_c \approx 1.93$ of Nb. Deviations from the model for the junctions with the largest d_1 are attributed to the fact that the Nb and Al are not fully in the dirty limit and d_1 is not small compared to the coherence length.

I. INTRODUCTION

The fabrication technology of Josephson tunnel junctions based on refractory superconductors, such as Nb and NbN, using artificial barriers, is well developed today.[1,2] It is well known that the electrical characteristics of these junctions display some characteristics features, of which the proximity knee is the most pronounced, which cannot be described in the framework of the standard tunnel theory for *SIS*- (superconductor-insulator-superconductor) type structures.[3,4] In the case of Nb technology the reason is that the dielectric barrier in such junctions is produced by the deposition of a thin layer of another material onto the lower electrode. For the overlayer material mostly Al is used, but also other metals have been investigated.[5,6] This layer is subsequently oxidized (or nitridized[7]) and often covered with a second thin Al layer. As a result some residual Al layers appear adjacent to the dielectric barrier and the tunnel structure is Nb/Al/Al-oxide/Al/Nb. Similar structures are created in the case of NbN junctions[8] or in the form of Nb/Al junctions sandwiched between NbN electrodes as in NbN/Nb/Al/Al-oxide/Al/Nb/NbN.[9] The NbN devices with a sputtered MgO barrier, which often suffer from layers with degraded superconducting properties adjacent to the barrier, can be modeled as NbN(I)/NbN(II)/MgO/NbN(II)/MgO(I) with T_c[Nb(II)] $< T_c$[Nb(I)].[10]

In all these cases the equivalent structure is $SS'IS''S$, where S' and S'' are thin layers of superconductors with lower critical temperature than that of the bulk electrode S, or normal-metal layers. The proximity effect between the S and S' metals influences the properties of the junction. In some practical applications such proximity layers may be used advantageously as, for example, in particle or phonon detectors, in which the reduced gap region adjacent to the junction barrier is used as a quasiparticle trap, in which excess quasiparticles are collected from the electrode.[11]

The properties of $SS'IS''S$ structures have been discussed theoretically in a number of works.[12–23] For the calculation of the tunnel current one should solve first the proximity effect problem of the SS' sandwich. The simplest approach is the McMillan proximity effect model.[12] This model assumes the presence of a supplementary potential barrier of low transparency at the SS' interface and small thicknesses of the S and S' layers compared to the coherence lengths of these materials. In Ref. 13 a model of the Josephson effect in *SNINS* junctions was developed using this method. However, in practical tunnel structures the assumptions of the McMillan model are mostly not fulfilled. The thickness of at least the S layer is generally much larger than the coherence length of S. Secondly, there is mostly an intimate contact between the S and S' layer.

In Refs. 14–16 a microscopic approach was developed

that is based on the calculation of the coordinate dependence of the Green's functions for arbitrary transparency of the SS' boundary. In these papers the order parameter was assumed to be spatially independent in S and S'. This approach is only valid under certain conditions for the parameters of the S and S' materials and the boundary transparency (see discussion below). In Ref. 17 a model was developed based on the quasiclassical Eilenberger equations,[24] which were solved in a self-consistent way, taking into account a spatial dependence of the order parameter. However this model is valid only if the S and S' materials are in the clean limit. Moreover, calculations of the tunnel current were not done, so that a comparison with experimental data for tunnel junctions is not possible yet. More recently, the proximity effect was discussed theoretically in the clean limit in the SN double layer[18] in the framework of the Gor'kov equations, as well as in SNS Josephson junction[19,20] in the framework of the Bogolubov–de Gennes equations. These theories, however, are not applicable for the real tunnel structures mentioned above.

Most Nb or NbN tunnel junctions are fabricated using room-temperature sputter deposition, creating polycrystalline films, which are in the dirty limit. Therefore our theoretical model is based on the assumption that the dirty limit condition holds for the S and the S' metal. For this case a microscopic theory was developed in Refs. 21 and 22 for $SN'IN''S$ junctions, i.e., for proximity layers with zero critical temperature. Recently this model was extended to account for a finite critical temperature of the S' layer.[23] The aim of the present paper is (a) to generalize the results of Refs. 21–23 to the case of finite SS' boundary resistance (i.e., for the existence of an additional potential barrier at the SS' interface); (b) to make a comparison between the theory and experimental data for Nb/Al/Al-oxide/Al/Nb tunnel junctions.

II. THE MODEL OF AN $SS'IS''S$ JUNCTION

We assume that one or both electrodes of the Josephson tunnel junction are formed by an SS' sandwich, while the transparency of the insulating layer is small enough to neglect the effect of the tunnel current on the superconducting state of the electrons. The SS' boundary can have arbitrary finite transparency, but which is large compared to the transparency of the junction barrier. Further we assume that the dirty limit condition holds for the S and S' materials, the critical temperature of the S' material, T_c^*, is less than that of the S metal, T_c, and the transverse dimensions of the junction are much less than the Josephson penetration depth, $W<\lambda_J$. Due to the last condition all quantities can be assumed to depend only on a single coordinate x normal to the interface surfaces of the materials.

We will consider below the most important practical case:

$$l \lesssim d \ll \xi^*, \quad d_s \gg \xi_s^* \gg l_s \ , \tag{1}$$

where $\xi^*=(D/2\pi T_c)^{1/2}$ and $\xi_s^*=(D_s/2\pi T_c)^{1/2}$ are the coherence lengths, l, l_s the electron mean free paths (mfp), d, d_s the thicknesses, and D, D_s the diffusion coefficients of the S' and S metals, respectively. ξ^* is related to the bulk coherence length $\xi_{s'}^*$ of the S' material by $\xi_{s'}^*=\xi^*(T_c/T_c^*)^{1/2}$. The coherence length ξ^* in the S' layer is defined such that in the following T_c^* can be treated as an independent variable. The first condition in (1) allows one to assume that all quantities within the S' layer are independent of x, while the second condition makes it possible to neglect the reduction of the critical temperature of the SS' electrode compared to that of a bulk S metal.

The low transparency of the junction barrier allows one to use the relations of the standard tunnel theory.[3,4] According to this theory, the current through the junction is determined by the retarded Green's functions $F_{1,2}(\varepsilon)$ and $G_{1,2}(\varepsilon)$ near the tunnel barrier. Here, the indices 1,2 refer to different electrodes of the junction. In the case of a large value of the McCumber parameter, $\beta_c \gg 1$, the voltage V across the junction is constant and the tunnel current density through the junction is determined by

$$J=\mathrm{Re}J_p(V)\sin\varphi+\mathrm{Im}J_p(V)\cos\varphi+\mathrm{Im}J_q(V) \ , \qquad \varphi=2eVt+\varphi_0 \ , \tag{2a}$$

where φ is the phase difference between the junction electrodes and φ_0 is an integration constant.

$$\mathrm{Re}J_p(V)=\frac{\sigma_n}{2e}\int_{-\infty}^{+\infty}d\varepsilon\tanh\left[\frac{\varepsilon}{2T}\right] \times[\mathrm{Im}F_1(\varepsilon)\mathrm{Re}F_2(\varepsilon+eV) +\mathrm{Re}F_1(\varepsilon+eV)\mathrm{Im}F_2(\varepsilon)] \tag{2b}$$

is the amplitude of the supercurrent,

$$\mathrm{Im}J_p(V)=\frac{\sigma_n}{2e}\int_{-\infty}^{+\infty}d\varepsilon\left[\tanh\frac{\varepsilon+eV}{2T}-\tanh\frac{\varepsilon}{2T}\right] \times\mathrm{Im}F_1(\varepsilon+eV)\mathrm{Im}F_2(\varepsilon) \tag{2c}$$

is the dissipative component of the current due to interference between the Cooper pairs and the quasiparticles, and

$$\mathrm{Im}J_q(V)=\frac{\sigma_n}{2e}\int_{-\infty}^{+\infty}d\varepsilon\left[\tanh\frac{\varepsilon+eV}{2T}-\tanh\frac{\varepsilon}{2T}\right] \times\mathrm{Re}G_1(\varepsilon)\mathrm{Re}G_2(\varepsilon+eV) \tag{2d}$$

is the quasiparticle current component. Here σ_n is the normal-state conductivity per unit junction area. The dirty limit condition makes it possible to assume that the functions $F_{1,2}(\varepsilon)$ and $G_{1,2}(\varepsilon)$ in Eqs. (2) are equal to their values at the $S'I$, respectively IS'', boundary, i.e., we ignore tunneling out of the bulk of the electrodes.

As noted in Ref. 21, the problem of determining the functions $G(\varepsilon)$ and $F(\varepsilon)$ entering into Eqs. (2) must be solved in two stages. First, it is necessary to determine the spatial dependence of the order parameter, $\Delta(x)$, in the SS' electrode. Then, by performing the analytical continuation from the Matsubara frequencies

$\omega_n = \pi T(2n+1)$ to the complex plane by the substitution $\omega_n = -i\varepsilon$, and using the solution $\Delta(x)$, one can calculate the functions $F(\varepsilon)$ and $G(\varepsilon)$ for a real energy ε.

Below we solve the proximity effect model formulated above. Some theoretical results obtained within this model for the case of vanishing SS' boundary resistance were discussed in Ref. 23.

III. PROXIMITY EFFECT IN THE SS' SANDWICH

With the assumptions given above the proximity effect in a system of two dirty metals can be described within the framework of the Usadel equations[25] for the S and S' layers (the domain $x \geq 0$ is occupied by the S metal, $-d \leq x < 0$ by the S' metal):

$$\left.\begin{aligned} &\Phi_s = \Delta_s + (\xi_s^*)^2 \frac{\pi T_c}{\omega G_s}[G_s^2 \Phi_s']', \quad G_s = \frac{\omega}{(\omega^2+\Phi_s^2)^{1/2}} \qquad (3a)\\ &\Delta_s \ln(T/T_c) + 2\pi T \sum_{\omega>0} \{(\Delta_s - \Phi_s G_s)/\omega\} = 0 \qquad (3b) \end{aligned}\right\} \quad x \geq 0 ,$$

$$\left.\begin{aligned} &\Phi = \Delta + (\xi^*)^2 \frac{\pi T_c}{\omega G}[G^2 \Phi']', \quad G = \frac{\omega}{(\omega^2+\Phi^2)^{1/2}} \qquad (4a)\\ &\Delta \ln(T/T_c^*) + 2\pi T \sum_{\omega>0} \{(\Delta - \Phi G)/\omega\} = 0 \qquad (4b) \end{aligned}\right\} \quad -d \leq x \leq 0 ,$$

where $\Phi = \omega F/G$, Φ_s $[F = \Phi/(\omega^2+\Phi^2)^{1/2}]$ and Δ, Δ_s are the modified Usadel functions and the order parameters in the S' and S materials, respectively. ω is the Matsubara frequency, $\omega_n = \pi T(2n+1)$ $(n = 0, 1, 2, \ldots)$, and the prime denotes differentiation with respect to the coordinate x. The properties of these equations are discussed extensively in Ref. 26.

Equations (3) and (4) must be supplemented with the boundary conditions in the bulk of the electrode:

$$\Phi_s(\infty) = \Delta_s(\infty) = \Delta_0(T) , \qquad (5)$$

as well as at the SS' boundary:[27]

$$\xi_s^* G_s^2 \Phi_s' = \gamma \xi^* G^2 \Phi', \quad \gamma = (\rho_s \xi_s^*)/(\rho \xi^*) , \qquad (6a)$$

$$\xi^* \gamma_{BN} G \Phi' = G_s(\Phi_s - \Phi), \quad \gamma_{BN} = R_B/\rho\xi^* , \qquad (6b)$$

and at the S' dielectric boundary:

$$\Phi'(-d) = 0 . \qquad (7)$$

Here $\Delta_0(T)$ is the BCS value of the order parameter of a homogeneous superconductor at the temperature T. ρ and ρ_s are the normal-state resistivities of the S' and S metal, whereas R_B is the product of the resistance of the SS' boundary and its area. The parameters γ and γ_{BN} have simple physical meanings. γ is a measure of the strength of the proximity effect between the S and S' metals, whereas γ_{BN} describes the effect of the boundary transparency between these layers.

In the first approximation in (d/ξ^*) one can neglect nongradient terms in Eq. (4a) and obtain $\Phi = A = \text{const}$, $\Delta = B = \text{const}$, if $d \ll \xi_\omega = \xi^*[\pi T_c/(\omega^2+\Phi^2)^{1/2}]^{1/2}$. Because of the condition $d \ll \xi^*$ this is true for frequencies $\omega \ll \Omega_d = \pi T_c(\xi^*/d)^2$. Then one can obtain in the next approximation by linearizing Eq. (4a)

$$\Phi'(x) = \frac{\omega}{\pi T_c} \frac{\Phi(0)-\Delta}{G(0)} \frac{x+d}{(\xi^*)^2}, \quad \omega \leq \Omega_d . \qquad (8)$$

Determining $\Phi'(0)$ from Eq. (8) and substituting the resulting equation into the boundary conditions Eqs. (6) we arrive at a boundary condition for the function Φ_s

$$\xi_s^* G_s \Phi_s'(0) = \frac{\gamma_m \tilde{\omega}\{\Phi_s(0)-\Delta\}}{\{1+\gamma_B^2(\tilde{\omega}^2+\tilde{\Delta}^2)+2\gamma_B G_s(0)[\tilde{\omega}+\tilde{\Phi}_s(0)\tilde{\Delta}/\tilde{\omega}]\}^{1/2}} , \qquad (9)$$

where $\tilde{\omega} = \omega/\pi T_c$, $\tilde{\Phi}_s = \Phi_s/\pi T_c$, $\tilde{\Delta} = \Delta/\pi T_c$, and

$$\gamma_m = \gamma \frac{d}{\xi^*}, \quad \gamma_B = \gamma_{BN} \frac{d}{\xi^*} , \qquad (10)$$

and a relation determining the function Φ

$$\Phi(x) = \Phi(0) = \frac{G_s(0)\Phi_s(0) + \gamma_B \tilde{\omega} \Delta}{G_s(0) + \gamma_B \tilde{\omega}}, \quad -d \leq x \leq 0 . \qquad (11)$$

The self-consistency equation in S, Eq. (3b), converges for frequencies $\omega \geq \pi T_c \ll \Omega_d$. Thus the boundary condition Eq. (9) in the frequency domain $\omega \ll \Omega_d$ is sufficient to solve the proximity effect problem in S, Eqs. (3), provided the order parameter Δ in S' is known. The latter can be found from the self-consistency equation (4b). Therefore, the SS' problem is described by γ_m, γ_B, and the ratio T_c^*/T_c, which is implicitly contained in Δ.

The dependence on T_c^*/T_c can be made explicit as follows. Note that in the limit of a thin S' layer, $d \ll \xi^*$, the two characteristic frequencies in Eqs. (4), $\Omega_c \approx \pi T_c$ and Ω_d, differ substantially: $\Omega_d \gg \Omega_c$. For $\omega \leq \Omega_d$ the relation between Δ and Φ is given by Eq. (8). However, the sum over ω in the self-consistency equation (4b) converges for $\omega > \Omega_d$, because in this limit one can neglect gradient terms in Eq. (4a) and obtain $\Phi = \Delta$. Thus, in order to find a relation between A and B, one should deter-

mine the function Φ also at higher frequencies, $\omega > \Omega_d$. For that, let us use the fact that for $\omega > \Omega_c$ and $\Delta = \text{const}$ Eq. (4a) can be linearized, giving the solution

$$\Phi = B + (A-B)\frac{\cosh[\beta(x+d)/\xi^*]}{\cosh[\beta d/\xi^*]}, \qquad \beta = \left[\frac{\sqrt{\omega^2+A^2}}{\pi T_c}\right]^{1/2}. \tag{12}$$

The solutions (8) and (12) match for $\Omega_c \ll \omega \ll \Omega_d$. Substituting (12) in (4b) and taking into account that

$$2\pi T \sum_{\omega>0} \frac{\cosh[\beta(x+d)/\xi^*]}{(\omega^2+A^2)^{1/2}\cosh[\beta d/\xi^*]} \approx \ln\left[\frac{2\gamma^*\Omega_d}{\pi T}\right] - 2\pi T \sum_{\omega>0}\left[\frac{1}{\omega} - \frac{1}{(\omega^2+A^2)^{1/2}}\right], \tag{13a}$$

where $\gamma^* \approx 1.78$ is the Euler's constant, we obtain a solution for the order parameter in the S' layer, Δ:

$$\Delta = B = A\left[\ln\left[\frac{2\gamma^*\Omega_d}{\pi T}\right] - \Sigma_1\right]\ln^{-1}\left[\frac{2\gamma^*\Omega_d}{\pi T_c^*}\right], \tag{13b}$$

$$\Sigma_1 = 2\pi T \sum_{\omega>0}\left[\frac{1}{\omega} - \frac{1}{(\omega^2+A^2)^{1/2}}\right]. \tag{13c}$$

Substituting Eqs. (11)–(13) in Eq. (9) one obtains the boundary condition for Φ_s:

$$\xi_s^* G_s(0)\Phi_s'(0) = \frac{\alpha\gamma_m\tilde{\omega}\Phi_s(0)}{\{1+2\alpha\gamma_B\tilde{\omega}G_s(0)+\alpha^2\gamma_B^2\tilde{\omega}^2\}^{1/2}}, \tag{14a}$$

where the parameter α is given by

$$\alpha = [\Sigma_1 + \ln(T/T_c^*)]/\ln(2\gamma^*\Omega_d/\pi T_c^*), \tag{14b}$$

and the function Φ is determined by

$$\Phi(x) = \Phi(0) = \frac{\Phi_s(0)}{1+\alpha\gamma_B[\tilde{\omega}^2+\tilde{\Phi}_s^2(0)]^{1/2}}. \tag{14c}$$

Thus the proximity effect problem in the SS' bilayer is reduced to the set of equations (3) for the S layer, with the boundary condition Eq. (14a), in which the parameter α, as given by Eq. (14b), is related to $\Phi_s(0)$ by Eqs. (13c) and (14c). There are three parameters which enter the problem: γ_m, γ_B, and the ratio of the critical temperatures T_c^*/T_c.

The problem can be simplified in the following limits: (1) for small values of the parameters γ_m and γ_B: $\gamma_m \ll 1$, $\gamma_B \ll 1$; (2) for large γ_m values: $\gamma_m \gg \max\{1;\gamma_B\}$; (3) for large γ_B values: $\gamma_B \gg \max\{1;\gamma_m\}$.

Let us discuss these limits separately.

A. The limit $\gamma_m \ll 1$, $\gamma_B \ll 1$

In order to relate the order parameter Δ to $\Phi_s(0)$ in this limit, the solution Φ in S' is matched to Φ_s in S as follows. Going over to the limit of small γ_m, it follows from Eq. (9) that

$$\xi_s^*\Phi_s'(0) = 0 \quad \text{for } \omega \ll \Omega_\gamma = \pi T_c/\gamma_m. \tag{15}$$

Since the sum in the self-consistency equation (3b) converges for frequencies $\omega < \Omega_c$ ($\Omega_c \ll \Omega_\gamma$) the functions Δ_s and Φ_s can be assumed to be spatially independent:

$$\Phi_s(x) = \Delta_s(x) = \Delta_0, \quad \omega \ll \Omega_\gamma. \tag{16}$$

Then Eq. (13b) reduces to $\Sigma_1 = \ln(T_c/T)$. In this limit the parameter α in Eq. (14b) is given by

$$\alpha = \ln(T_c/T_c^*)/\ln(2\gamma^*\Omega_d/\pi T_c^*) = \ln(T_c/T_c^*)/[\ln(2\gamma^*)+\ln(T_c/T_c^*)+2\ln(\xi^*/d)] \tag{17}$$

[$\ln(2\gamma^*) \simeq 1.27$]. From this equation it is seen that α reflects the influence of a finite T_c^* value on the proximity effect in the SS' sandwich.

Introducing the effective parameters

$$\gamma_m^{\text{eff}} = \alpha\gamma_m, \quad \gamma_B^{\text{eff}} = \alpha\gamma_B, \tag{18}$$

the problem has been reduced to the proximity effect in an SN sandwich with $T_c^* = 0$, as was derived in Ref. 22, but with the effective parameters γ_m^{eff} and γ_B^{eff} replacing the parameters γ_m and γ_B for the real SN sandwich. It is seen from Eqs. (17) and (18) that the thickness of the S' layer enters the problem in the form of the parameter $\gamma_m \sim d/\xi^*$ and in α by a small logarithmic correction. In what follows in this section we will neglect the latter correction. Then, for small γ_m and γ_B values, the number of parameters can be reduced to two: the effective proximity parameters γ_m^{eff} and γ_B^{eff}. The proximity effect is now described by the Eqs. (3), (16), and

$$\Phi = \Delta_0/[1+\gamma_B^{\text{eff}}\beta^2], \tag{19a}$$

$$\Delta = \Phi\ln\left[\frac{2\gamma^*\Omega_d}{\pi T_c}\right]\ln^{-1}\left[\frac{2\gamma^*\Omega_d}{\pi T_c^*}\right], \tag{19b}$$

where β, as given in Eq. (12), in this limit is reduced to the form $\beta = (\tilde{\omega}^2+\tilde{\Delta}_0^2)^{1/4}$, similar to that of the SN sandwich problem.[22]

In the considered limit of small γ_m, γ_B the functions Δ_s and Φ_s are determined in the first approximation by Eq. (16) and Φ and Δ by Eq. (19). In the next approximation in γ_m^{eff} and assuming $\gamma_B^{\text{eff}} = 0$ we have from Eqs. (3a) and (14a)

$$\Phi_s(x) = \Delta_0\{1-[C/(1+C)]\exp(-\beta x/\xi_s^*)\}, \tag{20}$$

where

$$C = \gamma_m^{\text{eff}}\beta/\{1+\gamma_B^{\text{eff}}\tilde{\omega}^2[2/\beta^2+\gamma_B^{\text{eff}}]\}^{1/2}$$

and $\beta = (\tilde{\omega}^2+\tilde{\Delta}_0^2)^{1/4}$.

It follows from Eqs. (14c) and (20) that

$$\Phi(0) \approx \Phi_s(0) \approx \Delta_0(1-C). \tag{21}$$

Equation (17) for the parameter α is approximate because rigid boundary conditions for the S layer, Eq. (16),

were assumed in its derivation. We have calculated α exactly as a function of T_c^*/T_c in the following way. The function $\Phi_s(x)$ was determined numerically using two different approaches: first, by solving the exact boundary value problem, Eqs. (3), (9), (11), and (13), and secondly in the framework of the "effective γ_m" approach by solving the Eqs. (3), (14a), and (18), assuming $T_c^*=0$. For both methods the parameter α was calculated as the ratio of the values of $\gamma_m^{\rm eff}$ and γ_m (for $\gamma_B=0$) which correspond to identical solutions $\Phi_s(x)$ in the limit $\gamma_m \ll 1$. For small values of $d/\xi^* \ll 1$ a good numerical fit for the dependence of α on T_c^*/T_c is given by

$$\alpha=\gamma_m^{\rm eff}/\gamma_m \approx \ln(T_c/T_c^*)/[2.9+\ln(T_c/T_c^*)+2\ln(\xi^*/d)]. \tag{22}$$

Equations (22) and (17) thus differ by the numerical coefficient in the denominator, which reflects the difference between the approximate solution (16) of Eq. (3a) and the exact one. Figure 1 shows the dependencies of α on T_c^*/T_c calculated from Eq. (22) for a number of values d/ξ^*. We note the following points: (a) The parameter α is small for $T_c^* \geq 0.1 T_c$ (which is the case for most practical materials). In the limit of very low values of T_c^*/T_c the parameter $\alpha=\gamma_m^{\rm eff}/\gamma_m$ goes to 1 very slowly. This implies that the finite T_c^* of the S' material has a large influence on the proximity effect, even if $T_c^* \ll T_c$. (b) The dependence of α on ξ^*/d is fairly weak. This property of the problem allows one to neglect the dependence of α on ξ^*/d for large values of this ratio. The main dependence on d/ξ^* is already taken into account by γ_m and γ_B, as defined in Eq. (10). In the following we will take as a typical value $d/\xi^* \approx 0.1$.

Let us consider separately the case of finite γ_B values (finite SS' boundary resistance). The solution in the S' layer is determined by Eq. (11). The latter relation allows one to derive the equations of the well-known McMillan model.[12] Substituting Eq. (11) into the Greens function $G=\omega/(\omega^2+\Phi^2)^{1/2}$, one obtains for the S' layer

$$G=\frac{Z(\omega)\omega}{[\varphi^2(\omega)+Z^2(\omega)\omega^2]^{1/2}}\ , \tag{23}$$

where

$$Z(\omega)=1+\frac{\Gamma Z_s(\omega)}{[\varphi_s^2(\omega)+Z_s^2(\omega)\omega^2]^{1/2}}\ , \tag{24a}$$

$$\varphi(\omega)=\Delta+\frac{\Gamma\varphi_s(\omega)}{[\varphi_s^2(\omega)+Z_s^2(\omega)\omega^2]^{1/2}}\ , \tag{24b}$$

$$\varphi_s(\omega)=\Delta_0,\quad Z_s(\omega)=1,\quad \Gamma=\pi T_c/\gamma_B\ . \tag{24c}$$

In this limit G_s and Φ_s are equal to their bulk values for all $x>0$. In the McMillan model the following two parameters are defined: $\Gamma_n=\hbar v_{Fn}D^*/4d$ and $\Gamma_s=\hbar v_{Fs}D^*/4d_s$, where D^* is the SN (SS') boundary transparency, and v_{Fn}, v_{Fs} are the Fermi velocities in the N (or S') and S layer. Equations (23) and (24) are equivalent to the McMillan equations with the identifications $\Gamma_n=\pi T_c/\gamma_B$ and $\Gamma_s=0$, which is true for $D^* \ll 1$ and large d_s. It can be shown that for thin S layers ($d_s \ll \xi_s^*$) the complete set of McMillan equations is obtained.[28]

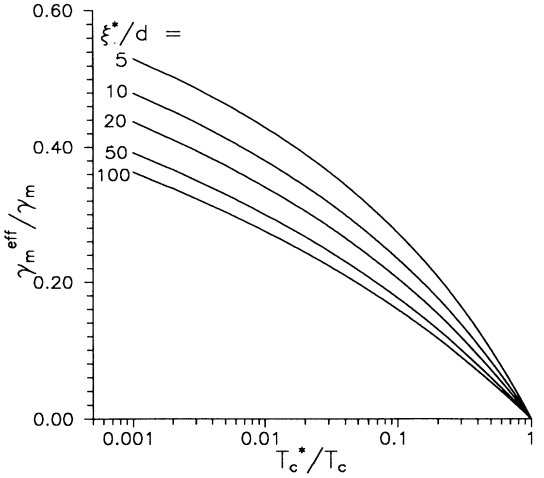

FIG. 1. Ratio of the effective proximity parameter $\gamma_m^{\rm eff}$ (for an SN sandwich with $T_c^*=0$) and the proximity parameter γ_m (for a sandwich with $T_c^* \neq 0$) as a function of the critical temperature ratio of the S' and S metal, T_c^*/T_c, for various thicknesses of the S' layer, ξ^*/d.

We note that the above approximation, Eqs. (16) and (20), of weak influence of the proximity effect on the properties of the S layer was discussed extensively in literature.[12–16] However, as was shown above, this limit corresponds to the case of small γ_m values only. In many practical cases (e.g., Nb/Al tunnel junctions) this limit is not satisfied. Below we solve the proximity effect model for other values of the parameters.

B. The limit $\gamma_m \gg \max\{1,\gamma_B\}$

As follows from the boundary conditions Eqs. (9)–(11), the functions Φ, and $\Phi_s(0)$ are determined by the following relation for frequencies $\omega \gg \pi T_c(1+\gamma_B)/\gamma_m$:

$$\Phi=\Phi_s(0)=\Delta_0'(T)\ , \tag{25a}$$

where $\Delta_0'(T)$ is the equilibrium BCS value of the order parameter in the S' layer. For temperatures $T \geq T_c^*$ Eq. (25a) leads to

$$\Phi=\Phi_s(0)=0\ . \tag{25b}$$

Equations (3) with the boundary conditions Eqs. (5) and (25b) were first solved in Ref. 26 for the SN sandwich problem. The behavior of Φ_s near the SS' boundary (for $0 \leq x \leq \xi_s^*$) is given by

$$\Phi_s(x)=B(T)x/\xi_s^*\ ,$$

$$B(T)=2T_c[1-(T/T_c)^2]/[7\zeta(3)]^{1/2}\ , \tag{26}$$

where $\zeta(x)$ is the Riemann ζ function, $\zeta(3)\cong 1.2$.

Substituting Eq. (26) in the boundary condition Eq. (14a) we have in the next approximation in γ_m^{-1}

$$B(T)=\alpha\gamma_m\tilde{\omega}\Phi_s(0)\{1+\alpha\gamma_B\tilde{\omega}(2+\alpha\gamma_B\tilde{\omega})\}^{-1/2}\ , \tag{27a}$$

$$\alpha=\left[\frac{7\zeta(3)}{8}[\Phi_s(0)/\pi T]^2+\ln(T/T_c^*)\right]/\ln(2\gamma^*\Omega_d/\pi T_c^*). \tag{27b}$$

For temperatures not too close to T_c^* one has $\ln(T/T_c^*)\gg(\Phi_s(0)/\pi T)^2$. Then it follows from Eqs. (27) that

$$\Phi_s(0)\approx\frac{B(T)}{\tilde{\omega}}\frac{\{1+\gamma_B^{\rm eff}\tilde{\omega}(2+\gamma_B^{\rm eff}\tilde{\omega})\}^{1/2}}{\gamma_m^{\rm eff}}\sim(T_c-T)\ . \tag{28}$$

Here the parameters $\gamma_m^{\rm eff}$, $\gamma_B^{\rm eff}$ are again given by Eq. (18), but now with α[Eq. (28)]=[$\ln(T/T_c^*)/\ln(T_c/T_c^*)$]$\alpha$[Eq. (17)], where α is explicitly temperature dependent. In the opposite case of temperatures close to T_c^* we obtain from Eqs. (27)

$$\Phi_s(0)\approx\pi T_c\left[\frac{8T^2B(T)}{7\zeta(3)\omega T_c^2\gamma_m}\ln(2\gamma^*\Omega_d/\pi T_c^*)\right]^{1/3}$$
$$\sim(T_c-T)^{1/3}\ . \tag{29}$$

It follows from Eqs. (27)–(29) and (14c) that the values of the functions Φ and $\Phi_s(0)$ decrease with increasing γ_m. The temperature and γ_m dependencies of Φ and $\Phi_s(0)$ are different in the regions $T\approx T_c^*$ and $T>T_c^*$. Namely, at high temperatures $\Phi\approx\Phi_s(0)\sim(T_c-T)/\gamma_m^{\rm eff}$ as is also the case for the SN sandwich.[23] At lower temperatures, $T_c^*\le T\le T^*$, where T^* is given by[23]

$$T^*=T_c^*\left\{1+\left[\frac{\ln(T_c/T_c^*)[(T_c/T_c^*)^2-1]}{2^{1/2}\pi\alpha\gamma_m}\right]^{2/3}\right\} \tag{30}$$

and α is given by Eq. (17), a crossover takes place to weaker dependencies of Φ and $\Phi_s(0)$ on T and γ_m: $\Phi_s(0)\sim\{(T_c-T)/\gamma_m\}^{1/3}$. As a result $\Phi_s(0)$ grows rapidly as temperature decreases and approaches T_c^* and finally Eq. (25a) holds when $T<T_c^*$. Therefore with decreasing temperature in the region $T\approx T^*$ the crossover takes place from proximity induced superconductivity in the S' layer (small values $\Phi\ll T_c^*$) to the superconducting state in the S' layer due to the pair-potential Δ_0' (large values $\Phi\sim T_c^*$).

C. The limit $\gamma_B\gg\max\{1;\gamma_m\}$

In this limit the S and S' layers are nearly decoupled and we obtain in the first approximation

$$\Phi_s(x)=\Delta_0(T),\quad 0<T<T_c\ , \tag{31a}$$

$$\Phi=\begin{cases}\Delta_0'(T), & 0<T<T_c^*,\\ 0, & T_c^*<T<T_c\ .\end{cases} \tag{31b,c}$$

In the next approximation the function Φ at $T_c^*<T<T_c$ is finite and is given by Eq. (14c) with $\Phi_s=\Delta_0(T)$, where the parameter α should be determined self-consistently from Eqs. (13b) and (14b), 14(c). Proceeding in this way, we obtain the following equation for α (provided $\alpha\gamma_B\tilde{\omega}\gg1$):

$$\alpha=\left[\ln(T/T_c^*)+(T/T_c)\frac{\tilde{\Delta}_0^2(T)}{\alpha^2\gamma_B^2}\sum_{\omega}\frac{1}{\tilde{\omega}^3(\tilde{\omega}^2+\tilde{\Delta}_0^2)}\right]/\ln(2\gamma^*\Omega_d/\pi T_c^*)\ . \tag{32}$$

Let us analyze in more detail the case when $T_c^*/T_c\ll1$. Evaluating the sum in Eq. (32) we find the crossover temperature

$$T^*\approx T_c^*\left\{1+K\left[\frac{(T_c/T_c^*)\ln(T_c/T_c^*)}{\alpha\gamma_B}\right]^{2/3}\right\}. \tag{33}$$

where $K=[7\zeta(3)/8]^{1/3}\approx1.016$ and α is given by Eq. (17). If $T>T^*$ the second term in square brackets in Eq. (32) is small compared to $\ln(T/T_c^*)$ and the parameter $\alpha=\alpha$[Eq. (28)] as in the limit of large γ_m. We regain Eq. (19) but now in the limit of large γ_B, so that Φ is reduced to

$$\Phi=\frac{\Delta_0(T)}{\gamma_B^{\rm eff}(\tilde{\omega}^2+\tilde{\Delta}_0^2)^{1/2}}\ . \tag{34}$$

In the opposite case of temperatures close to T_c^*, i.e., for $T_c^*<T<T^*$, the function Φ is again given by Eq. (34), but with a reduced $\gamma_B^{\rm eff}$ in comparison with Eq. (28):

$$\gamma_B^{\rm eff}=K\left[\gamma_B\alpha\frac{(T_c/T_c^*)^2}{\ln(T_c/T_c^*)}\right]^{2/3}, \tag{35}$$

where α is given by Eq. (17). Therefore with decreasing temperature in the region $T\simeq T^*$ the proximity induced superconductivity in the S' layer, Φ, is increased. Such a behavior of the function Φ is qualitatively similar for both cases of large γ_m and large γ_B values. Below we illustrate it by numerical calculations.

D. Arbitrary γ_m, γ_B, and T_c^*/T_c

For arbitrary temperature and values of γ_m, γ_B, and T_c^*/T_c Eqs. (3) and (4) with boundary condition (9) were solved numerically by a self-consistent procedure, taking into account the spatial variation of the order parameter $\Delta_s(x)$, as well as of the Usadel functions $\Phi_s(x)$ and $G_s(x)$. On each iteration step the self-consistency equation (4b) for Δ was solved using the relations (11) and (13) between Δ, Φ, and Φ_s (see the Appendix).

In Fig. 2 the spatial dependencies of Δ_s and Δ are presented for $T_c^*/T_c=0.3$, $T\ll T_c^*$ and (a) for different values of γ_m and $\gamma_B=0$ and (b) for different values of γ_B and $\gamma_m=1$. It is seen that the order parameters in the S and S' layers at the SS' interface differ even for vanishing SS' boundary transparency ($\gamma_B=0$) as must be expected from the fact that the coupling constants in the S and S' metals are different. In the case of $\gamma_m\gg(1+\gamma_B)$ (large

conductivity of S' material), the order parameter near the SS' boundary, $\Delta_s(0)$, is strongly suppressed due to the proximity effect. With an increase of γ_B the jump in the order parameter at the boundary increases and $\Delta_s(x)$ becomes spatially independent. This is the range where the McMillan model is applicable. In the limit $\gamma_B \to \infty$ the S and S' layers become decoupled and then $\Delta = \Delta_0'(T)$, $\Delta_s = \Delta_0(T)$.

In Figs. 3(a) and 3(b) the temperature dependencies of Δ and $\Delta_s(0)$ for $T_c^*/T_c = 0.3$ are shown. Note the crossover in the behavior of $\Delta(T)$ at $T \approx T_c^*$ for large γ_m and γ_B parameters. As is seen from Fig. 3(a), in the case of zero boundary resistance ($\gamma_B = 0$) the order parameter in S', Δ, is almost equal to the order parameter in S near the SS' boundary, $\Delta_s(0)$, and the difference between Δ_s and Δ becomes smaller as γ_m increases. In the limit of large γ_m (curve d) the order parameters Δ and Δ_s are equal in accordance with Eq. (25) and behave nearly like the equilibrium order parameter in S', $\Delta_0'(T)$. Further at large γ_m and decreasing temperature Δ and $\Delta_s(0)$ grow rapidly near the crossover temperature T^*/T_c^* (≈ 0.36 for $\gamma_m = 100$) in accordance with Eq. (30). This behavior is seen in Fig. 3 as a positive curvature of the $\Delta(T)$ and $\Delta_s(T)$ curves.

As is seen from Fig. 3(b), an increase of γ_B results in an increase of the jump of the order parameter at the SS' boundary [see also Fig. 2(b)]. In the limit of large γ_B one sees a crossover to the behavior described by Eq. (31): the curve for $\Delta_s(T, \gamma_B = 100)$ nearly coincides with

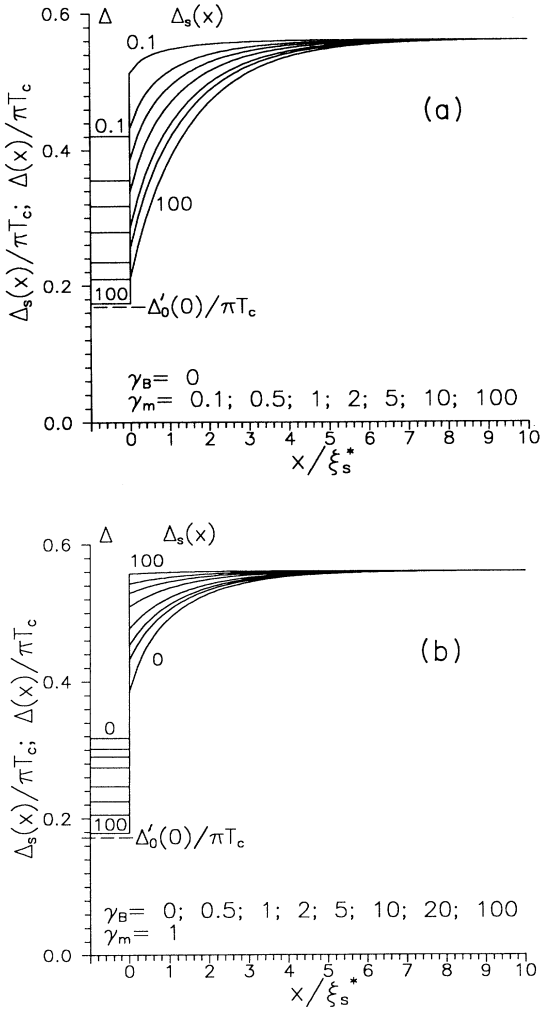

FIG. 2. Spatial dependence of the order parameter Δ_s in S (for $x > 0$) and Δ in S' ($x < 0$), for an SS' sandwich with $T_c^*/T_c = 0.3$, at temperature $T \ll T_c^*$: (a) for $\gamma_B = 0$, γ_m ranging from 0.1 to 100; (b) for $\gamma_m = 1$, γ_B ranging from 0 to 100. The bulk value of the order parameter $\Delta_0(0)$ in S is reached for large x. That for S' is indicated by $\Delta_0'(0)$.

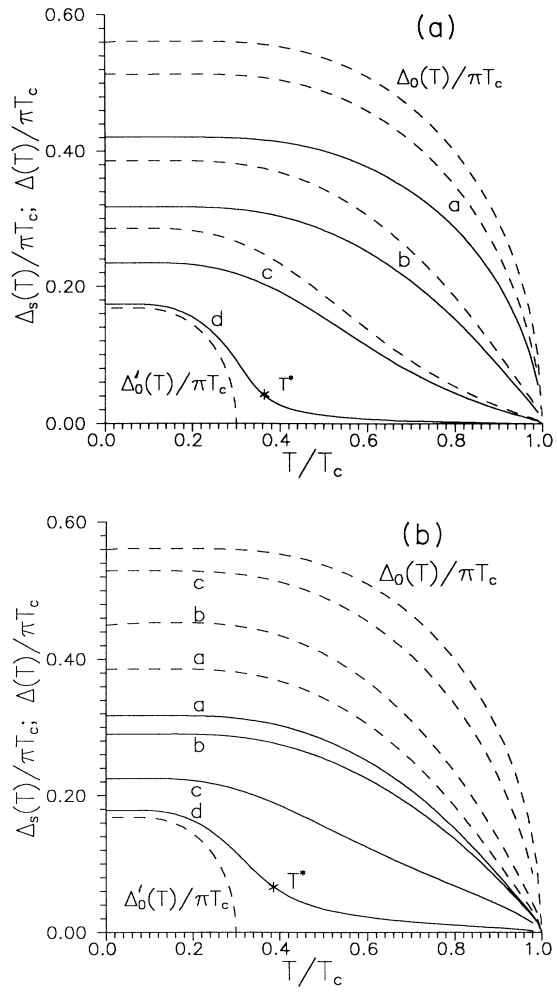

FIG. 3. (a) Temperature dependence of the order parameter Δ_s in S at the SS' interface ($x = 0$) (dashed curves) and of Δ in S' (solid curves), for an SS' sandwich with $T_c^*/T_c = 0.3$, $\gamma_B = 0$, and $\gamma_m = 0.1$ (a); 1 (b); 5 (c); 100 (d). In case (d) the curves for Δ_s and Δ merge. The crossover temperature T^* for $\gamma_m = 100$ [Eq. (30)] is indicated in the corresponding curve. The BCS curves for the S' and S layer are indicated with $\Delta_0'(T)$ and $\Delta_0(T)$. (b) As (a) for $\gamma_m = 1$ and $\gamma_B = 0$ (a); 1 (b); 10 (c); 100 (d) [Δ_s coincides with $\Delta_0(T)$]. In case (d) the curve for Δ_s practically merges with $\Delta_0(T)$. The crossover temperature T^* for $\gamma_B = 100$ [Eq. (33)] is indicated in the corresponding curve.

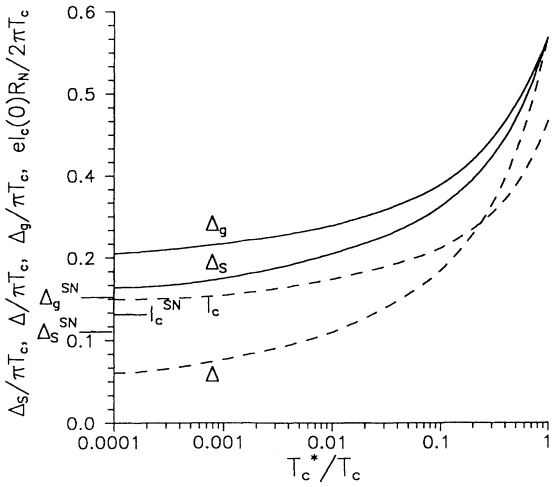

FIG. 4. Dependence on the critical temperature ratio T_c^*/T_c of an SS' sandwich with $\gamma_m=1$, and $\gamma_B=0$ and at $T\ll T_c$ of the order parameter $\Delta_s(0)$ in S at the SS' interface ($x=0$); Δ in S'; the gap energy Δ_g; and the critical current $I_c(0)$ of a symmetrical $SS'IS'S$ junction. In the limit $T_c^*=0$ (SN sandwich) the values $\Delta_s(0)=\Delta_s^{SN}$, $\Delta=\Delta^{SN}=0$, $\Delta_g=\Delta_g^{SN}$, and $I_c=I_c^{SN}$ are reached.

$\Delta_0(T)$ and $\Delta(T,\gamma_B=100)$ is close to $\Delta_0'(T)$. As in the case of large γ_m a positive curvature is present in the $\Delta(T)$ dependence at the crossover temperature $T^*/T_c^*\approx 0.38$ (for $\gamma_B=100$) in accordance with Eq. (33).

The dependence of the order parameters Δ and $\Delta_s(0)$ on the ratio T_c^*/T_c, at $T\ll T_c$, is shown in Fig. 4 for $\gamma_m=1$, $\gamma_B=0$. It is seen that in accordance with the weak (logarithmic) dependence of $\gamma_m^{\rm eff}$ on T_c/T_c^* [see Eq. (22)] the order parameter $\Delta_s(0)$ exceeds its value for $T_c^*=0$ (Δ_s^{SN}, indicated in the figure, corresponding to the case of the SN sandwich) even for small values of T_c^*/T_c. The same effect occurs for the order parameter in the S' region, Δ, where in the SN-case $\Delta^{SN}=0$.

IV. THE DENSITIES OF STATES

In order to calculate the normalized density of states in the electrodes, $N(\varepsilon,x)$, for arbitrary values of T_c^*/T_c and γ_m,γ_B it is convenient to introduce a new function Θ_s by the relations $\Phi_s=\omega\tan\Theta_s$, $G_s=\cos\Theta_s$ and then to carry out the substitution $\omega=-i\varepsilon$. Equation (3a) is then rewritten as

$$\Theta_s''(\varepsilon,x)+i\tilde{\varepsilon}\sin\Theta_s(\varepsilon,x)+\tilde{\Delta}_s(x)\cos\Theta_s(\varepsilon,x)=0\ . \tag{36a}$$

The boundary condition in the bulk of the S electrode, Eq. (5), becomes

$$\Theta_s(\varepsilon,\infty)=\arctan[i\tilde{\Delta}_0(T)/\tilde{\varepsilon}]\ , \tag{36b}$$

and the boundary conditions at the SS' boundary, Eqs. (9) and (11), take, respectively, the form

$$\Theta_s'=-\frac{\gamma_m[\tilde{\Delta}\cos\Theta_s+i\tilde{\varepsilon}\sin\Theta_s]}{[1+\gamma_B^2(\tilde{\Delta}^2-\tilde{\varepsilon}^2)+2\gamma_B(\tilde{\Delta}\sin\Theta_s-i\tilde{\varepsilon}\cos\Theta_s)]^{1/2}}\ , \tag{36c}$$

$$\tan\Theta=\frac{\sin\Theta_s+\gamma_B\tilde{\Delta}}{\cos\Theta_s-i\gamma_B\tilde{\varepsilon}}\ . \tag{36d}$$

Here the function Θ in S' is defined analogous to Θ_s in S, $\tilde{\varepsilon}=\varepsilon/\pi T_c$, $\tilde{\Delta}_s(x)=\Delta_s(x)/\pi T_c$ and the distance is normalized to ξ_s^*. The frequency-independent functions Δ and $\Delta_s(x)$ are already known from the solution of the stationary problem.

The quasiparticle densities of states in the S and S' layers are then determined by the following relations:

$$N_s(\varepsilon,x)=\mathrm{Re}G_s=\mathrm{Re}(\cos\Theta_s)\ , \tag{37a}$$

$$N(\varepsilon,x)=\mathrm{Re}G=\mathrm{Re}(\cos\Theta)\ . \tag{37b}$$

Let us first consider some limiting cases.

For small values of γ_m and $\gamma_B=0$ and using the simple solution Eq. (21) and Eqs. (37), we obtain for the densities of states at the SS' boundary in the S layer and in the S' layer

$$N_s(\varepsilon,x=0)=N(\varepsilon)=\mathrm{Re}\left[\frac{-i\varepsilon(1+\gamma_m^{\rm eff}\beta_\varepsilon)}{\{\Delta_0^2(T)-\varepsilon^2(1+\gamma_m^{\rm eff}\beta_\varepsilon)^2\}^{1/2}}\right]\ , \tag{38}$$

where $\beta_\varepsilon=(\tilde{\Delta}_0^2-\tilde{\varepsilon}^2)^{1/4}$. It follows from Eq. (38) that the function $N(\varepsilon)$ has two singularities: one for $\varepsilon=\Delta_0$ and another for

$$\varepsilon=\Delta_g=\Delta_0\{1-2^{1/3}(\gamma_m^{\rm eff})^{4/3}\tilde{\Delta}^{2/3}\}\ . \tag{39}$$

Equation (39) determines an energy gap at the SS' boundary. Note that comparing Eq. (39) with the corresponding one for an energy gap suppression in the presence of Abrikosov-Gorkov type pair breaking,[29]

$$\Delta_g=\Delta_0(1-\zeta^{2/3})^{3/2}\ , \tag{40}$$

one can relate the $\gamma_m^{\rm eff}$ parameter to an effective pair-breaking rate ζ. For $T=0$, using the relation $\Delta_0(0)/\pi T_c=\gamma^*/\pi$, we have

$$\zeta\equiv(\tau\Delta_0)^{-1}=2^{1/2}(\tfrac{2}{3})^{3/2}\frac{\gamma^*}{\pi}(\gamma_m^{\rm eff})^2\ . \tag{41}$$

The singularity in the density of states, given by Eq. (38), at $\varepsilon=\Delta_0$ is rather weak: $N(\varepsilon)\sim(\varepsilon^2-\Delta_0^2)^{1/8}$ and is smeared out in the next approximation in $\gamma_m^{\rm eff}$.

For finite γ_B and $\gamma_m/(1+\gamma_B)\ll 1$ the density of states is given by Eqs. (23) and (24) with $\omega=-i\varepsilon$ and Eq. (37) (McMillan model with $\Gamma_n=\pi T_c/\gamma_B$ and $\Gamma_s=0$). In that case the densities of states in the S and S' layers differ strongly. The former, $N_s(\varepsilon)=\varepsilon/(\varepsilon^2-\Delta_0^2)$, $\varepsilon>\Delta_0$ coincides in this approximation with the BCS density of states. The function $N(\varepsilon)$ has two singularities, one at $\varepsilon=\Delta_0$: $N(\varepsilon)\sim(\varepsilon^2-\Delta_0^2)^{-1/2}$ and another at $\varepsilon=\Delta_g$: $N(\varepsilon)\sim(\varepsilon^2-\Delta_g^2)$, where the energy gap Δ_g for small Γ_n is related to the equilibrium values of the order parameters in the S and S' layers, Δ_0 and Δ_0', by the simple relation

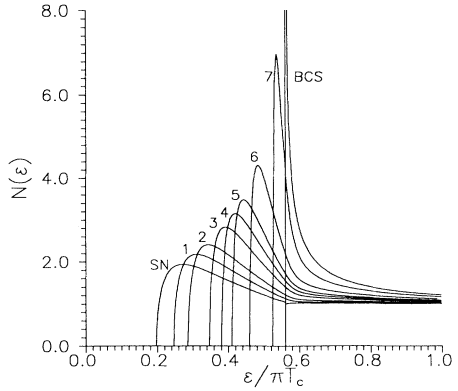

FIG. 5. Normalized density of states in S', $N(\varepsilon)$, at $T=0$, of an SS' sandwich with $\gamma_m=1$, $\gamma_B=0$, and $T_c^*/T_c=0$ for the SN sandwich (SN); 10^{-3} (1); 10^{-2} (2); 0.1 (3); 0.2 (4); 0.3 (5); 0.5 (6); 0.8 (7); and 1 for the BCS-case (BCS).

$$\Delta_g=\Delta_0'+\Gamma_n\left[\frac{\Delta_0-\Delta_0'}{\Delta_0+\Delta_0'}\right]^{1/2}. \tag{42}$$

For finite γ_B both singularities in $N(\varepsilon)$, as well as the one in the $N_s(\varepsilon)$ are smeared out. This behavior was studied in detail for the case of the SN sandwich in Ref. 22.

For arbitrary temperatures and values of T_c^*/T_c, γ_m, and γ_B the problem was solved numerically. The results of the calculations for $N(\varepsilon)$ in S' in the low-temperature limit $T=0$ for $\gamma_m=1$ and $\gamma_B=0$, are shown in Fig. 5 for different values of T_c^*/T_c [because $\gamma_B=0$, $N(\varepsilon)=N_s(\varepsilon,x=0)$]. It is seen that with increasing T_c^*/T_c ratio the energy gap increases and a sharp singularity in $N(\varepsilon)$ appears at $\varepsilon<\Delta_0$ in accordance with Eq. (39), until for $T_c^*/T_c=1$ the BCS density of states is obtained. It is important to note that this singularity leads to the knee structure in the current-voltage characteristics of a $SS'IS''S$ junction (see below).

Figure 6 shows the densities of states in the S and S' layers at the SS' interfaces for finite γ_B and different γ_m values in the low-temperature limit, $T=0$. In this case $N(\varepsilon)$ and $N_s(\varepsilon)$ differ strongly. For small γ_m two singularities exist in $N(\varepsilon)$, as was discussed above. For sufficiently large γ_m the peak at $\varepsilon=\Delta_0$ is smeared out. The density of states in the S layer, $N_s(\varepsilon)$, at small γ_m values goes almost like a BCS curve. At large γ_m the energy gap decreases and a large number of states appears at energies $\varepsilon<\Delta_0$. We note that, as was discussed above, in the considered limit of small SS' boundary transparency (large γ_B) and small γ_m, the behavior of the densities of states in S and S' layers is qualitatively similar to the predictions of the McMillan model. However, for other values of the parameters our model gives results which differ considerably.

It is important to note that, as is seen from comparison

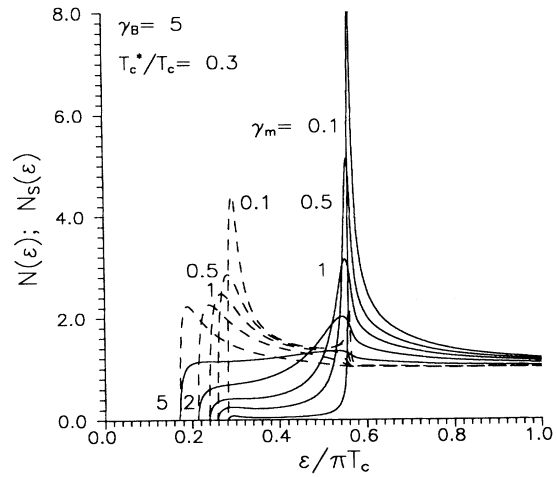

FIG. 6. Normalized densities of states in S' (dashed curves) and S at the SS' interface (solid curves) at $T=0$, for $T_c^*/T_c=0.3$, $\gamma_B=5$, and $\gamma_m=0.1$; 0.5; 1; 2; and 5.

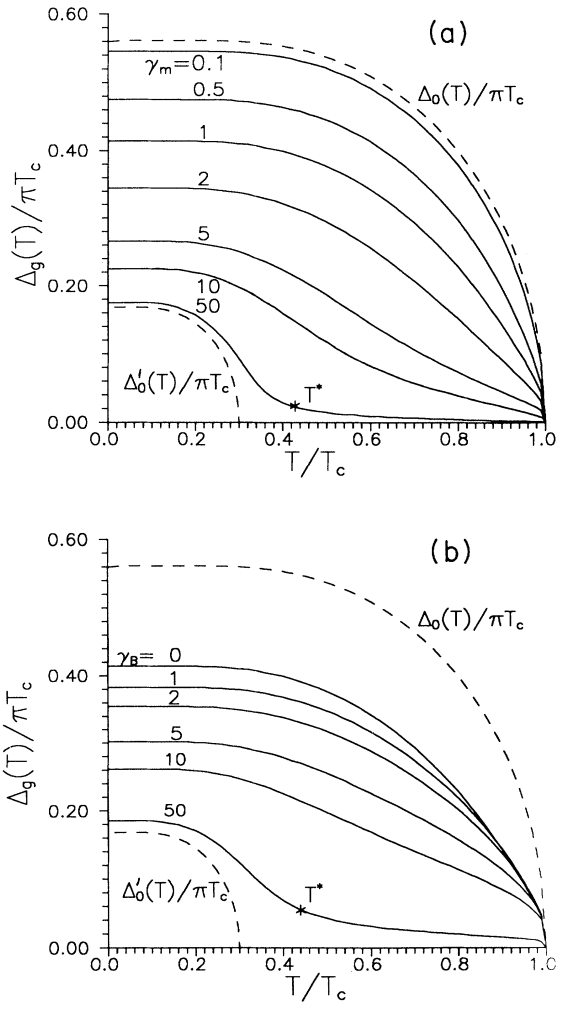

FIG. 7. Energy gap in the density of states in an SS' sandwich as a function of temperature. $T_c^*/T_c=0.3$, for (a) γ_m ranging from 0.1 to 50 and $\gamma_B=0$ and (b) $\gamma_m=1$ and γ_B ranging from 0 to 50. The crossover temperatures T^* [Eq. (30), respectively, (33)] for $\gamma_m=50$, respectively $\gamma_B=50$, are indicated in the corresponding curve. The bulk energy gaps of S and S' are given by the dashed curves $\Delta_0(T)$ and $\Delta_0'(T)$, respectively.

of the Figs. 5 and 6, the densities of states in S' differ qualitatively for the cases of zero and finite γ_B values (vanishing and finite SS' boundary resistance). Namely, in the latter case the density of states $N(\varepsilon)$ has a two-peak structure for small γ_m values.

The energy gap of the density of states in the S' region, Δ_g, is also of interest because it is directly reflected in the current-voltage characteristic (CVC) of a junction. We have calculated $\Delta_g(T)$ for $T_c^*/T_c=0.3$ and a number of γ_m, γ_B values. The results are shown in the Figs. 7(a) ($\gamma_B=0$, $\gamma_m=0,\ldots,50$) and 7(b) ($\gamma_m=1$, $\gamma_B=0,\ldots,50$). It is seen that for small values of γ_m and γ_B the function $\Delta_g(T)$ is close to the BCS curve, $\Delta_0(T)$. Large modifications take place for large values of γ_m, γ_B and a positive curvature is seen, as discussed above for Figs. 3. This behavior is a result of the crossover at temperature T^* from proximity-induced superconductivity in the S' layer above T^* to the superconducting state in S' below T^*, due to the pair potential $\Delta_0'(T)$.

The dependence of Δ_g on the T_c^*/T_c ratio in the low-temperature limit, $T=0$, is shown in Fig. 4 for $\gamma_m=1$ and $\gamma_B=0$. It is seen that even for extremely low ratio $T_c^*/T_c\sim10^{-4}$ the magnitude of Δ_g exceeds its limiting value Δ_g^{SN} which corresponds to $T_c^*=0$ (SN bilayer). In the practically most interesting region, $T_c^*/T_c\sim0.1-1$, the gap Δ_g depends considerably on the T_c^*/T_c ratio and at $T_c^*=T_c$ equals the bulk gap in S: $\Delta_g=\Delta_0(0)$.

V. CRITICAL CURRENT OF *SS'IS'S* JUNCTION

To calculate the critical current of an $SS'IS''S$ junction it is convenient to rewrite the expression (2b) for $eV=0$ in the Matsubara representation

$$\frac{eI_cR_N}{2\pi T_c}=\frac{T}{T_c}\sum_{\omega>0}\omega^{-2}\Phi_1(0)G_1(0)\Phi_2(0)G_2(0)\ , \tag{43}$$

where the indices 1, 2 refer to the different electrodes.

Let us first limit ourselves to the case $\gamma_B\ll1$ and to a symmetrical junction. For small values of γ_m (Eqs. (21) and (43) lead to Eq. (31) of Ref. 23, with the limiting values (the limiting values given in Ref. 23 are numerically not correct)

$$\begin{aligned}\frac{eI_cR_N}{2\pi T_c}&=\frac{\Delta_0^2(T)}{8T_c^2}[1-\gamma_m^{\rm eff}4(2-1/\sqrt{2})\zeta(3)/\pi^2]\\&\approx\frac{\Delta_0^2(T)}{8T_c^2}(1-1.2\gamma_m^{\rm eff})\end{aligned} \tag{44}$$

at $T\approx T_c$, and

$$\begin{aligned}\frac{eI_cR_N}{2\pi T_c}&=\frac{\Delta_0(0)}{4T_c}\left[1-\gamma_m^{\rm eff}\left[\frac{\Delta_0(0)}{T_c}\right]^{1/2}\frac{\sqrt{2}\{\Gamma(\frac{1}{4})\}^2}{3\pi^2}\right]\\&\approx0.44(1-0.84\gamma_m^{\rm eff})\ ,\end{aligned} \tag{45}$$

for $T\ll T_c$, using, $\Gamma(1/4)\simeq3.626$. The BCS relation $\Delta(0)/T_c\simeq1.76$ was assumed in Eqs. (44) and (45).

In the opposite case of large γ_m values and $T>T^*$ we have from Eq. (28)

$$\frac{eI_cR_N}{2\pi T_c}=\frac{\pi^2}{96}\frac{T_c}{T}\left[\frac{B(T)}{T}\frac{1}{\gamma_m^{\rm eff}}\right]^2\sim(T_c-T)^2\ , \tag{46}$$

where the temperature T^* is given by Eq. (30). The dependence $(T_c-T)^2$ close to T_c is typical for proximity effect junctions independent of the T_c^*/T_c ratio. On the other hand, as follows from Eq. (29), the temperature dependence in the interval $T_c^*<T<T^*$ is $I_cR_N\sim(T_c-T)^{2/3}$. At $T<T_c^*$ in this large γ_m limit I_c is determined by the Ambegaokar-Baratoff[30] (AB) expression with $\Delta_0'(T)$ replacing $\Delta_0(T)$. Therefore, an enhancement of I_c below $T\approx T^*$ takes place.

For finite γ_B values, $\gamma_B\gg\max\{1;\gamma_m\}$ we have from Eqs. (43) and (34)

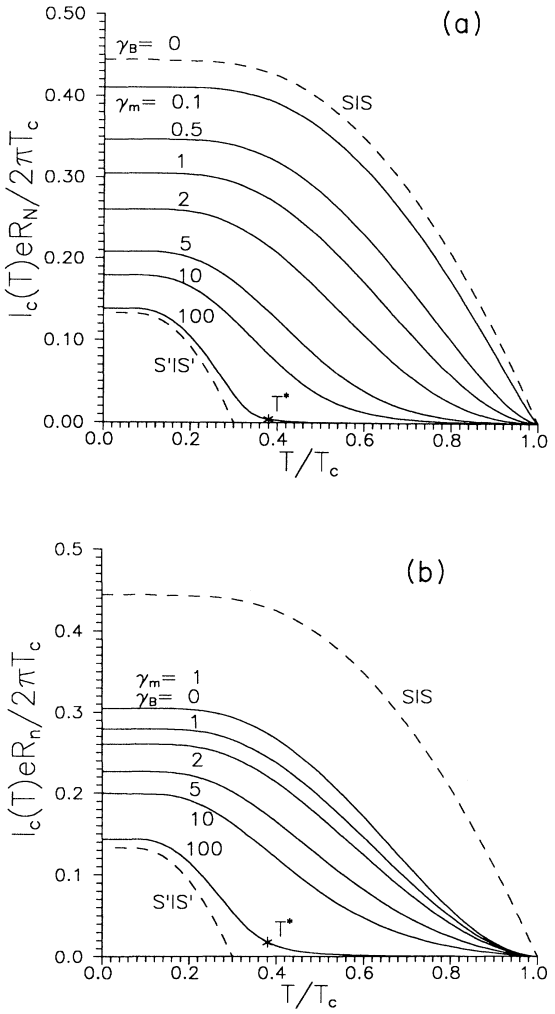

FIG. 8. Critical current $I_c(T)$ as a function of temperature for a symmetrical $SS'IS'S$ junction with $T_c^*/T_c=0.3$ for (a) γ_m ranging from 0.1 to 100 and $\gamma_B=0$; and (b) $\gamma_m=1$ and γ_B ranging from 0 to 100. The AB (dashed) curves for an SIS and $S'IS'$ junction, as well as the crossover temperatures T^* [Eq. (30), respectively Eq. (33)] for $\gamma_m=100$, respectively $\gamma_B=100$, are indicated.

$$\frac{eI_cR_N}{2\pi T_c} \approx \begin{cases} [\Delta_0'(T)/4T_c]\tanh[\Delta_0'(T)/2T], & 0<T_c<T^*, \quad (47a) \\ \pi/(2\gamma_B^{\rm eff}), & T_c^*<T_c\ll T, \quad (47b) \\ \pi^2 T_c\Delta_0^2/[48T^3(\gamma_B^{\rm eff})^2], & T\approx T_c\ . \quad (47c) \end{cases}$$

For arbitrary values of γ_m and T_c^*/T_c the dependencies $I_c(T)$ were calculated numerically using the solutions for Φ and G. The results are shown in Figs. 8(a) and 8(b) for $T_c^*/T_c=0.3$ and different γ_m and γ_B values. The positive curvature of $I_c(T)$, typical for the proximity effect junctions,[21-23] is seen at temperatures near T_c for finite values of the parameter γ_m. At sufficiently large γ_m Eq. (46) gives the behavior $I_c(T)\sim(T_c-T)^2$. For both cases of large γ_m and large γ_B the critical current $I_c(T)$ is given by the AB theory for an $S'IS'$ junction.

The dependencies of $I_c(T=0)$ on the ratio T_c^*/T_c are shown separately in Fig. 4 for $\gamma_m=1$ and $\gamma_B=0$. Analogous to the behavior of Δ_g, Δ_s, and Δ considered above, the reduced critical current $eR_NI_c/2\pi T_c$ saturates very slowly at small T_c^*/T_c ratio to its limiting value $eR_NI_s^{SN}/2\pi T_c$ corresponding to $T_c^*=0$ (SN bilayer). At $T_c^*\to T_c$ the magnitude of $\gamma_m^{\rm eff}$ goes to zero in accordance with Eq. (17) and the current $I_c\to I_c^{\rm AB}$.

VI. CURRENT-VOLTAGE CHARACTERISTICS

Using the solutions of the proximity effect problem for the SS' sandwich one can calculate the tunnel current according to Eq. (2). Here we discuss the results for the quasiparticle component of the current, $\mathrm{Im}J_q(V)$, as given by Eq. (2d).

The current-voltage curves (CVC) for a symmetrical $SS'IS'S$ junction for $T\ll T_c^*$ and $\gamma_m=1$, $\gamma_B=0$ are shown in Fig. 7 of Ref. 23 for different T_c^*/T_c ratios. There the crossover is shown between the cases of a SNINS junction with $T_c^*=0$ and of an ideal SIS junction with $T_c^*=T_c$. The variation of the ratio T_c^*/T_c leads to qualitative changes in the CVC's. In particular, with the increase of T_c^*/T_c a knee structure develops in the region $eV\approx 2\Delta_g$. The origin of this structure is the sharp singularity in the density of states $N(\varepsilon)$ at $\varepsilon<\Delta_0$ as shown in Fig. 5. Namely, the quasiparticles with energy in the interval $\Delta_g<\varepsilon<\Delta_0$ give a large contribution to the tunnel current at voltage $eV\approx 2\Delta_g$ leading to the knee on the CVC. The shape and the height of the knee depends on the T_c^*/T_c ratio, i.e., on the $\gamma_m^{\rm eff}$ value.

In Fig. 9 of Ref. 23 the calculated CVC's of symmetrical Nb/Al, Al oxide/Al/Nb junctions at $T=4.2$ K are presented for $\gamma_B=0$ and various values of γ_m. Both the gap voltage $eV=2\Delta_g(T)$ and the knee feature on the CVC depend strongly on the value of the γ_m parameter. At very large γ_m the gap value is reduced, the knee structure disappears and a crossover to a purely resistive CVC takes place. At small γ_m there exist a sharp knee structure. The height of the knee is maximal for $\gamma_m\simeq 0.2$. With further decrease of γ_m the gap Δ_g goes to the bulk gap of the S material, Δ_0, and the knee structure gradually disappears. It is seen from comparison of the Figs. 7 and 9 of Ref. 23 that variation of the T_c^*/T_c ratio for a fixed value of γ_m leads to qualitatively similar modifications of the CVC as with variation of γ_m for fixed T_c^*/T_c ratio. This is in accordance with the concept of the "effective γ_m" proximity effect parameter.

The modifications of the CVC of an SNINS Josephson junction ($T_c^*=0$) due to a finite SN boundary resistance, i.e., finite γ_B values, were discussed theoretically in Ref. 22. As was mentioned above, in most practically used $SS'IS''S$ Josephson junctions the influence of the boundary resistance of the SS' (and SS'') interfaces on the CVC is relatively small. Therefore we will not discuss here the behavior of CVC of the $SS'IS''S$ junction for finite γ_B.

Below we will compare the results of calculations with the experimental data of Nb/Al tunnel junctions.

VII. EXPERIMENTAL RESULTS

A. Device fabrication

We applied the model developed in the foregoing sections to describe the electrical characteristics of a series of $Nb_1/Al_1/Al$ oxide/$Al_2/Nb_2/Nb_2$ Josephson tunnel junctions, that were fabricated with different thicknesses d_1 of the base-electrode Al layer (ranging from 5 to 40 nm) and a constant thickness d_2 of the counterelectrode Al layer (nominally 3 nm). The indices 1 and 2 refer to the base- and counterelectrode, respectively. The multilayer was deposited in a single vacuum run using dc-magnetron sputtering on a water-cooled thermally oxidized Si substrate and structured by liftoff. Thermal oxidation at room temperature of the Al_1 layer was used to form the barrier with a current density of about 100 A/cm^2. The junctions were structured with the selective niobium anodization process (SNAP)[31] to have dimensions of 20×20 up to 200×200 μm^2. The Nb base-electrode thickness d_{s1} is 300 nm. The Nb counterelectrode was made in two steps. The first Nb_2 layer of 30 nm is part of the multilayer. After the anodization step a thick layer (200–500 nm) was deposited and structured by liftoff to form the counterelectrode and the contact leads.

B. Parameter estimates

For comparison of the model with the measurements we discuss the conditions of applicability. For Nb sputtered at low temperatures the electron mean free path (mfp) l_s is largely determined by the grain size,[32] which in our devices is approximately 20 nm as was seen from TEM analysis.[33] The coherence length ξ_s^* is then estimated as $\xi_s^*\approx[l_s\xi_s(0)/3]^{1/2}\approx 16$ nm, where $\xi_s(0)\approx 38$ nm is the clean limit value for Nb.[34] Thus the Nb layers obey the condition Eq. (1), $d_s\gg\xi_s^*$, but instead of the dirty limit condition $l_s\ll\xi_s^*$ we have $l_s\approx\xi_s^*$. For thick sputter deposited Al films we find from resistivity measurements mfp's of about 100–150 nm. Using $l\approx 100$ nm the coherence length of Al is estimated as $\xi_{s'}^*\approx 230$ nm [with $\xi_{s'}(0)\approx 1.6$ μm],[34] thus $\xi^*\approx 86$ nm, with $T_c(\mathrm{Al})=1.3$ K and $T_c(\mathrm{Nb})=9.3$ K. Thus $l\approx\xi^*$ and the Al is not in the dirty limit and secondly d_1 is not small

compared to ξ^* for the largest d_1 values. However, from our TEM analysis it was observed that the grain structure of the Al_1 layer reproduces that of the underlying Nb. If the mfp in the Al_1 layer is also limited by the grain size we even find a coherence length ξ^* as small as 38 nm. In that case $l<\xi^*$, but not $d_1 \ll \xi^*$ for the largest d_1 values and the thin S'-layer approximation is violated for even smaller d_1. For estimating the proximity parameters we rewrite γ [Eq. (6a)] as $\gamma=(\rho_s D_s^{1/2}/\rho D^{1/2}) =(D/D_s)^{1/2}[N(0)/N_s(0)]$, using $\rho^{-1}=e^2 DN(0)$. The diffusion coefficient is $D=\frac{1}{3}v_F^* l$, with v_F^* the effective Fermi velocity which can be obtained from the clean limit values of the coherence lengths,[34] using the BCS relation $\xi(0)=\hbar v_F^*/\pi\Delta(0)$. The normal-state electron densities of states at the Fermi energy are obtained from Ref. 35, γ_m/d is estimated as approximately 0.021 nm^{-1}, independent of the mfp in the Al.

The parameter γ_{BN} [Eq. (6b)] can be written as $\gamma_{BN}=(2l/3\xi^*)\{R^*/[(p_{Fs}/p_{Fs'})^2 D^*]\}$.[27] In the free-electron model the transmission coefficient D^* (related to the reflection coefficient R^* as $D^*=1-R^*$) for the transmission of a quantum-mechanical particle through the interface of two metals with different Fermi-velocities, is given by $D^*=1-R^*=(4v_{Fs}^* v_{Fs'}^*)/[(v_{FS}^*+v_{Fs'}^*)^2+4U_0^2]$.[17] U_0 is the height of a δ-potential barrier at the interface $U(x)=U_0\delta(x=0)$. If one takes only the mismatch in Fermi velocities into account always large D^* are obtained (≥ 0.85) for realistic v_F^* values of metals. Therefore in practice some additional barrier has to be taken into account to explain the lower transmission coefficients measured. More realistic models for D^* have been discussed by Wolf and Arnold.[15] In the literature a D^* value of about 0.4 is reported for Nb/Cu interfaces,[36] indicating that the transmission coefficient is not only due to the mismatch in Fermi velocities. Although all layers, apart from the Nb_2' layer, are deposited without vacuum break, so that there is an intimate contact between the Nb and Al layers, it is expected that there is a potential barrier present at the Nb/Al interfaces, decreasing the value of D^*. Using the literature value of D^* for the Nb/Cu interface we find for the Nb/Al interfaces $\gamma_B/d \approx 0.010$ nm^{-1} (independent of l). As was seen from the numerical results the influence of nonzero γ_B values on the electrical characteristics becomes only noticeable for γ_B values of the order of 1 or larger. The estimated γ_B/d value is fairly small and the effect of the finite γ_B value is therefore probably only noticeable for the largest d_1 values.

Because of the two-step fabrication process of the counterelectrode, we have to discuss its properties separately. The Al_2 layer starts to grow on the amorphous Al oxide and has a very fine polycrystalline structure with grain size of about 5 nm as seen from TEM pictures.[33] Since the 30-nm Nb_2 layer starts to grow on this Al layer it must be expected that its conductive properties are degraded, especially near to the Al_2/Nb_2 interface, due to the short mfp in the initial growth phase. Secondly, the Nb_2 layer is exposed to processing chemicals and atmosphere before the thick Nb_2' layer is deposited, so that it is oxidized at the Nb_2/Nb_2' interface. Despite the fact that this interface is sputter-cleaned before deposition of the Nb_2' layer it was found from current-voltage measurements that the conductivity of this interface is much less than that of bulk Nb. This implies that the γ_B value of the Nb_2/Nb_2' interface is probably not very small. Furthermore it was found from critical current and sum-gap versus temperature measurements that the critical temperature T_c^{exp} of some of the junctions is slightly reduced compared to the bulk value of Nb ($T_c=9.3$ K). We ascribe this to a relative poor quality of the Nb_2 layer. This may give rise to an additional proximity layer, creating a $S''S'S$-sandwich counterelectrode with $T_c^{**}(Al_2) < T_c^*(Nb_2) < T_c(Nb_2')$. These considerations all indicate that the gap reduction in the counterelectrode is larger than one may expect from the thickness d_2 of the counterelectrode Al layer. It is also expected that the counterelectrode gap value varies from sample to sample due to different aging and preparation conditions before the Nb_2' layer is deposited.

C. Measurements and discussion

The different junctions were characterized with current-voltage, critical-current, and sum-gap versus temperature measurements.

The sum gap, $V_g=(\Delta_{g1}+\Delta_{g2})/e$, and difference gap voltage $V_d=|\Delta_{g1}-\Delta_{g2}|/e$, were determined from the current-voltage characteristics (CVC) at low temperatures (1.1–1.6 K), where the gap energies have no temperature dependence. V_g was determined as the intersection of the tangent on the low-current part of the sharp current rise of the CVC with the voltage axis, whereas V_d was identified with the peak in the subgap current, eventually after subtraction of an ohmic leakage current.

In Fig. 9 the experimentally determined Δ_{g1} and Δ_{g2} are given as function of the thickness d_1. The experimen-

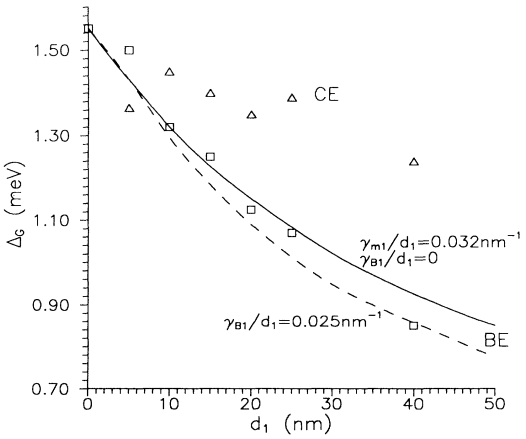

FIG. 9. Experimentally determined gap voltages of base (□) and counter (△) electrodes of Nb/Al_1, Al oxide, Al_2/Nb junctions as a function of the thickness d_1 of the Al_1-layer and constant Al_2-layer thickness. (——) Theoretical fit of base-electrode data with $\gamma_{m1}/d_1=0.032$ nm^{-1}, $\gamma_{B1}=0$. (— — —) the same, with $\gamma_{m1}/d_1=0.032$ nm^{-1} and $\gamma_{B1}/d_1=0.025$ nm^{-1}.

tal data $\Delta_{g1}(d_1)$ were fitted for small d_1 (where the influence of a finite γ_B is smallest) with the theoretical dependence $\Delta_g(\gamma_m(d),\gamma_B=0)$ (full curve), assuming Δ_0 to be equal to the bulk value for Nb, 1.55 meV. We find $\gamma_{m1}/d_1 \approx 0.032$ nm^{-1}, which is close to the estimated value. The gap reduction for small d_1 is well described by this curve. It is seen that the Δ_{g1} value for the junction with $d_1=40$ nm is considerably smaller than predicted by this curve. Ascribing the (extra) gap reduction due to a finite γ_B and fitting to the $\Delta_{g1}(40\text{ nm})$ data point gives $\gamma_{B1}\approx 1$ ($\gamma_{B1}/d_1 \approx 0.025$ nm^{-1}) using the γ_{m1}/d_1 value from the former fit. The dashed curve gives the Al-thickness dependence of the gap for these γ_{m1}/d_1 and γ_{B1}/d_1 values. However, now the gap values for the smaller d_1 values are slightly underestimated. The experimental value for γ_{B1}/d_1 indicates that the Nb/Al interface transparency is largely determined by an additional potential barrier. For D^* we obtain the value 0.21, which is fairly much smaller than the value found for Nb/Cu interfaces.[35]

The calculated γ_{m1}/d_1 value is considered to be a good estimate of the experimentally determined value 0.032 nm^{-1}, taking into account the uncertainties in materials parameters. However, the experimentally determined γ_{B1}/d_1 value is probably slightly overestimated and consequently the transmission coefficient D^* somewhat underestimated, because for at least the largest Al_1-layer thicknesses the model assumptions, and especially the thin-S' layer approximation, are not strictly fulfilled anymore. For large d_1 the order parameter in the S' layer decreases when approaching the $S'I$ interface, giving rise to an additional gap reduction, which therefore cannot only be ascribed to an SS' interface potential barrier.

Figure 10 shows the CVC's of a set of junctions, measured at 1.4 K with current bias. The voltage axis is normalized with $\Delta_0^{\rm exp}=1.93k_BT_c^{\rm exp}$ found for Nb from tunneling measurements on high-quality junctions with very thin Al layers[37,38] and in accordance with the used values

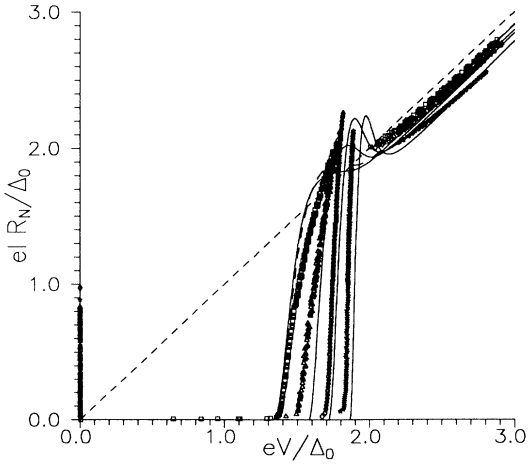

FIG. 10. Experimental current-voltage characteristics of Nb/Al_1, Al oxide, Al_2/Nb junctions at 1.4 K for $d_1=40$ (□), 25 (△), 15 (◇), and 5 nm (*), respectively, for the curves from left to right. (——) Theoretical curves using the γ_m values determined from Fig. 9 and $\gamma_{B1}=\gamma_{B1}=0$. (— — —) The same for junction with $d_1=40$ nm with $\gamma_{B1}=1$.

for Δ_0 and T_c for bulk Nb. The current axis is normalized with $\Delta_0^{\rm exp}$ and $R_N^{\rm fit}$ obtained by fitting the experimental data to the theoretical (solid) curve calculated with the γ_m values, determined from Fig. 9, taking $\gamma_{B1}=\gamma_{B2}=0$, at $eV/\Delta_0^{\rm exp}=2.75$. The differences in calculated and measured sum-gap voltages are fairly small and are largely ascribed to calibration errors of the measuring setups and errors in the estimates of the scaling parameters. For small d_1 the slope of the CVC at the sum-gap voltage and the height of the proximity knee is fairly well described with the model. The gap width increases with increasing d_1 more than predicted and the proximity knee remains more pronounced. The height of the proximity knee reaches a maximum (for $d_1=15$ nm), a feature which is also seen in Fig. 9 of Ref. 23. Taking into account the correction with nonzero γ_{B1} gives only marginal changes in the CVC (given by the dashed curve for the 40-nm junction with $\gamma_{B1}=1$; this curve largely merges with the curve for $\gamma_{B1}=0$). There are several possible explanations for the differences between theory and experiment. The shape of the CVC and especially the proximity knee is very sensitive to the exact energy dependence of the quasiparticle density of states: (a) The theoretical curves have been calculated under the assumption that the electrode metals consist of weak-coupling superconductors, whereas for Nb and Al Δ_0/k_BT_c values of about 1.93, respectively 2.1, instead of the BCS value 1.76, have been reported,[37,38] indicating strong-coupling effects. Indeed it has been shown recently that an SIS junction made up of strong-coupling materials shows also a proximity knee, contrary to an SIS junction with weak-coupling electrodes.[39] More important reasons are probably that the model assumptions, i.e., (b) the dirty limit conditions for the electrode materials and (c) the thin-S'-layer approximation, are not rigorously fulfilled. Using the dirty limit conditions implies that the densities of states, as calculated from the Usadel equations (especially the densities of states at the barrier, which are reflected in the tunneling measurements), do not depend on the direction of the electron trajectory. In the clean limit, however, only quasiparticles with a trajectory within a narrow cone, directed perpendicular to the SS' interface, can cross this interface and create the proximity effect, whereas the other quasiparticles are described by Φ functions which resemble those of the bulk (BCS) properties of the S, respectively S', metal. Both the affected and unaffected Φ functions go into the describing equations (in this case the Eilenberger equations[24]) so that it must be expected that the resulting tunneling densities of states show more BCS-like behavior than in the dirty limit. Another way of describing this is that in the clean case the quasiparticles not only tunnel from nearby the barrier interfaces but also from deeper out of the electrodes, where the densities of states are more BCS-like. The proximity effect in clean-limit proximity sandwiches is subject of further study.[40] Aspect (c) implies that for large S'-layer thicknesses the density of states in the S' layer at the SS' interface is strongly different from the BCS density of states, but changes gradually to more BCS-like, for increasing distance from the SS' interface.

Figures 11 and 12 show the measured temperature dependence of the sum-gap voltage $V_g(T)$ and the critical current $I_c(T)$ of these junctions, normalized with $T_c^{\rm exp}$, $\Delta_0^{\rm exp}$, and $R_N^{\rm fit}$, as well as the theoretical curves (solid lines), calculated with the same γ_m values as used for the CVC's and $\gamma_B=0$.

For low temperatures we find a close correspondence between measured and calculated $V_g(T)$ data within measurement and scaling errors. This means that the gap reduction in our junctions can be attributed largely to the proximity effect. For higher temperatures and larger Al layer thicknesses the experimental data are above the calculated curves. In fact all curves are BCS-like as is demonstrated in the inset of Fig. 11 by scaling the curves to $V_g(T=0)$. This means that the tunneling densities of states have energy gaps with BCS-like temperature dependence. The fact that for nonzero γ_B the density of states in the S' layer becomes more BCS-like, since the layers become decoupled, can only explain a small fraction of the difference between theory and experiment. The BCS-like temperature dependence suggests again that the devices do not fully obey the model assumptions, i.e., the dirty limit condition and the thin-S'-layer approximation.

For the normalization of the calculated critical-current curves one has to take into account explicitly the strong-coupling correction. The measured critical current values at low temperatures are fairly well described by the calculated values, corrected for strong-coupling effects, although they are for nearly all devices systematically slightly lower. This difference is ascribed to factors that decrease the critical current as, e.g., noise, RF interference, and not-complete suppression/cancellation of magnetic fields. Again we find that at higher temperatures and with increasing d_1 the critical currents are larger than predicted. The dashed curve in the main figure calculated with $\gamma_{B1}=1$ for the 40-nm junction shows that a nonzero γ_B gives only a marginal increase of I_c at these temperatures. Thus a nonzero γ_B value cannot explain the differences between theory and experiment. The inset shows the $I_c(T)$ curves normalized to the critical current measured at about 1.4 K, the lowest temperature in these measurements, being about equal to $I_c(0)$. For the junctions with the thinnest Al_1 layers $I_c(T)/I_c(0)$ is close to the Ambegaokar-Baratoff temperature dependence of a symmetrical junction with weak-coupling electrodes (indicated by BCS). For the 40-nm junction the temperature dependence deviates more from the AB dependence and is described better by the proximity model, as given by the curve labeled "40 nm." We see these aspects again as indications that the model assumptions are not fully fulfilled by these devices.

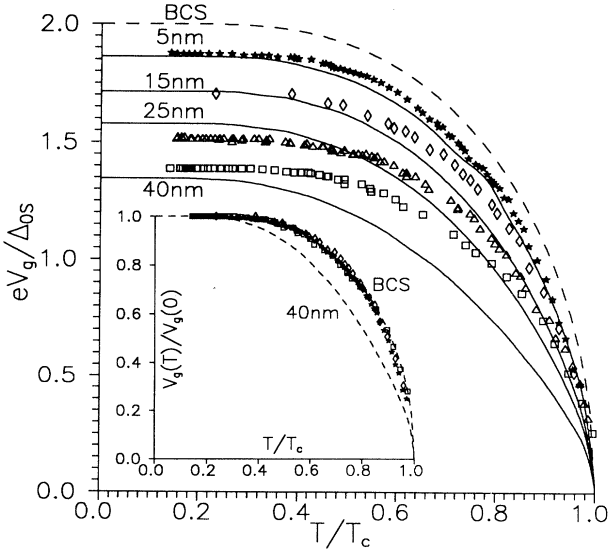

FIG. 11. Sum-gap voltage versus reduced temperature for Nb/Al_1, Al oxide, Al_2/Nb junctions for $d_1=5$ (*), 15 (◇), 25 (△), and 40 nm (□). The inset gives the sum-gap voltage normalized on the voltage at zero temperature.

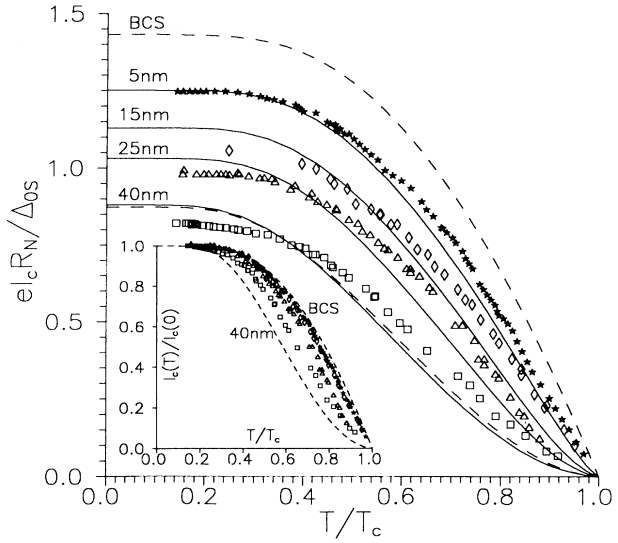

FIG. 12. Critical current versus reduced temperature for Nb/Al_1, Al oxide, Al_2/Nb junctions for $d_1=5$ (□), 15 (◇), 25 (△), and 40 nm (□). The inset gives the critical current normalized on the current at zero temperature.

In the foregoing we have shown that it is possible to describe the various experimentally determined electrical characteristics of the Nb/Al proximity junctions consistently in terms of the microscopic proximity developed in this paper, using only the proximity parameters γ_m/d and γ_B/d as fitting parameters. The values of these parameters used are close to the values estimated from material parameters. This supports the validity of the model. CVC, $I_c(T)$, and $V_g(T)$ measurements have been described simultaneously and consistently over the whole temperature range $T=0-T_c$ and for a fairly large range of proximity layer thicknesses with a proximity effect model, using in essence only two parameters.

The discrepancies between theory and experiment, as discussed above extensively, show how sensitive the electrical characteristics are to any differences in the densities of states, as, for example, due to long electron mfp's (instead of the dirty limit assumed in the discussed model) or due to the violation of the thin-S'-layer approximation

(used in this model). For a detailed quantitative description for these cases new models are needed.

VIII. CONCLUSIONS

A microscopic model of the proximity effect in a SS' sandwich of two superconducting metals S and S' (with $T_c > T_c^*$) in the dirty limit has been developed, which is applicable for thin S' layers backed by a thick S layer and for arbitrary transparency of the SS' interface. The proximity effect is described with three parameters: γ_m and γ_B, which are measures of the strength of the proximity effect and the interface transparency respectively, and the critical temperature ratio T_c^*/T_c.

In the limit of small γ_m it is shown that the dependence on T_c^*/T_c can be incorporated in effective proximity parameters $\gamma_m^{\rm eff}=\alpha(T_c^*/T_c)\gamma_m$ and $\gamma_B^{\rm eff}=\alpha(T_c^*/T_c)\gamma_B$.

A very remarkable difference between the proximity effect in SS' sandwiches with that in SN sandwiches ($T_c^*=0$) is that at all temperatures T ($<T_c$), also for $T>T_c^*$, the order parameter in the S' layer is nonzero, contrary to the SN case, where Δ_N is always zero. This effect causes large quantitative differences in the density of states in the S' layer, depending on the T_c^*/T_c value, and consequently in the energy gap in the density of states that is measured in the S' layer.

For small γ_m and nonzero γ_B (i.e., not perfect SS' interface transparency) the order parameter in S and S' is practically constant, as is required for the McMillan tunneling approach of the proximity effect. It is shown explicitly that in this case the equations can be recast in the form of the McMillan model.

For large values of γ_m and/or γ_B one sees qualitatively the same behavior, namely proximity-induced superconductivity above a certain crossover temperature T^* ($T_c \geq T^* > T_c^*$) and a nearly fully developed superconducting state for $T<T^*$ in the S' layer.

Using the solutions of the order parameter and densities of states in both proximity sandwich electrodes the electrical characteristics of $SS'IS''S$ Josephson tunnel junctions have been calculated as a function of T and γ_m. These characteristics show the typical features of experimental curves as measured on, for example, Nb/Al junctions. The most pronounced effects are the proximity knee and decreasing sum-gap voltage and a current rise at the sum gap which becomes more sloped with increasing γ_m.

The microscopic model was applied to describe the energy-gap reduction in a series of Nb/Al junctions with different Al-layer thicknesses of the base electrode (5–40 nm). In this way we determined the values $\gamma_m/d=0.032$ nm^{-1} and $\gamma_B/d=0.025$ nm^{-1}. The estimate from material parameters of the first parameter (0.021 nm^{-1}) is close to the experimentally determined value. The γ_B/d value found is considered to determine an upper limit of the SS' interface potential barrier, giving $D^*\approx 0.21$ as a lower estimate of the interface transparency. The current-voltage characteristics and the temperature dependence of the sum-gap voltage and the Josephson current were measured for all the junctions. These data could be described quantitatively fairly well with the model, using the small strong-coupling correction $\Delta_0/k_BT_c=1.93$ for Nb and the γ_m values, as determined from the gap reduction, without any other correction and/or scaling factors. The discrepancies found (a more pronounced proximity knee and more BCS-like temperature dependence of the sum-gap voltage and critical current than predicted for the junctions with the thickest Al layers) are largely attributed to the facts that (a) the metals of the junction are not fully in the dirty limit and (b) the proximity layers are not thin compared to the coherence length of the largest S'-layer thicknesses, as required by the model.

ACKNOWLEDGMENTS

These investigations in the program of the Foundation of Fundamental Research on Matter (FOM) have been supported by the Netherlands Technology Foundation (STW). A.A.G. and M.Yu.K. acknowledges support from the International Science Foundation Grant No. MDP000.

APPENDIX

In order to calculate $\Delta_s(x)$, Δ, $\Phi_s(\omega,x)$, and $\Phi(\omega)$ for arbitrary values of γ_m, γ_B, and T_c^*/T_c, the set of Usadel equations (3) was solved numerically by a self-consistent procedure, taking into account the boundary conditions (5) and (9) and the relation (11). The Usadel equations in the S region [Eq. (3)] are rewritten as

$$\Theta_s''+\tilde{\Delta}_s\cos\Theta_s-\tilde{\omega}\sin\Theta_s=0\ , \tag{A1}$$

$$\tilde{\Delta}_s\ln\frac{T}{T_c}+\frac{2T}{T_c}\sum_n\left\{\frac{\tilde{\Delta}_s}{\tilde{\omega}}-\sin\Theta_s\right\}=0\ , \tag{A2}$$

where the function Θ_s has been introduced by the relations $\tilde{\Phi}_s=\tilde{\omega}\tan\Theta_s$ and $G_s=\cos\Theta_s$. Here and in the following energies are normalized to πT_c (indicated by the tilde above the symbol) and distances to ξ_s^*.

The boundary conditions for Θ_s are obtained from Eqs. (5) and (9):

$$\Theta_s(\infty)=\arctan(\tilde{\Delta}_0/\tilde{\omega})\ , \tag{A3a}$$

$$\Theta_s'(0)=\gamma_m\frac{\tilde{\omega}\sin\Theta_s(0)-\tilde{\Delta}\cos\Theta_s(0)}{\{1+\gamma_B^2(\tilde{\omega}^2+\tilde{\Delta}^2)+2\gamma_B[\tilde{\omega}\cos\Theta_s(0)+\tilde{\Delta}\sin\Theta_s(0)]\}^{1/2}}\ , \tag{A3b}$$

The order parameter Δ in S' is determined by the self-consistency Eq. (4b) and relation (11):

$$\tilde{\Delta}\ln\frac{T}{T_c^*}+2\frac{T}{T_c}\sum_n\left\{\frac{\tilde{\Delta}}{\tilde{\omega}}-\sin\Theta(0)\right\}=0\ , \tag{A4}$$

$$\tan\Theta=\frac{\sin\Theta_s(0)+\gamma_B\tilde{\Delta}}{\cos\Theta_s(0)+\gamma_B\tilde{\omega}} . \tag{A5}$$

Equations (A4) and (A5) are combined to give

$$\tilde{\Delta}\ln\frac{T}{T_c^*}+2\frac{T}{T_c}\sum_n\left\{\frac{\tilde{\Delta}}{\tilde{\omega}}-\left[1+\left[\frac{\cos\Theta_s(0)+\gamma_B\tilde{\omega}}{\sin\Theta_s(0)+\gamma_B\tilde{\Delta}}\right]^2\right]^{-1/2}\right\}=0 . \tag{A6}$$

The sum over n in Eq. (A6) can be rewritten as

$$\sum_0^\infty\{\cdots\}=\sum_0^{\tilde{\Omega}_d}\{\cdots\}+\sum_{\tilde{\Omega}_d}^\infty\left[\frac{\tilde{\Delta}}{\tilde{\omega}}-\frac{\tilde{\Delta}}{[\tilde{\omega}^2+\tilde{\Delta}^2]^{1/2}}\right] , \tag{A7}$$

because for $\tilde{\omega}>\tilde{\Omega}_d=(\xi^*/d)^2$ we have $\Phi=\Delta$, i.e., $\Theta=\arctan(\Delta/\omega)$. The symbol $\{\cdots\}$ in Eq. (A7) denotes the expression in angular brackets in Eq. (A6).

Finally $\tilde{\Delta}$ is determined by the following recurrency expression:

$$\tilde{\Delta}^{(m+1)}=\frac{\frac{2T}{T_c}\left\{\sum_0^{\tilde{\Omega}_d}\left[1+\left[\frac{\cos\Theta_s^{(m)}(0)+\gamma_B\tilde{\omega}}{\sin\Theta_s^{(m)}(0)+\gamma_B\tilde{\Delta}^{(m)}}\right]^2\right]^{-1/2}+\sum_{\tilde{\Omega}_d}^{\tilde{\Omega}_{\max}}\frac{\tilde{\Delta}^{(m)}}{[\tilde{\omega}^2+(\tilde{\Delta}^{(m)})^2]^{1/2}}\right\}}{\ln(T/T_c^*)+(2T/T_c)\sum_0^{\tilde{\Omega}_{\max}}\frac{1}{\tilde{\omega}}} \tag{A8}$$

on the mth iteration step. Here $\tilde{\Omega}_{\max}$ is some cutoff frequency, $\tilde{\Omega}_{\max}>\tilde{\Omega}_d$. According to BCS theory the largest frequency that can occur is the Debye frequency Ω_D, thus $\Omega_{\max}=\Omega_D$.[28]

The order parameter in S, Δ_s, is determined simultaneously from Eq. (A2):

$$\tilde{\Delta}_s^{(m+1)}(x)=\frac{\frac{2T}{T_c}\sum_0^{\tilde{\Omega}_{\max}}\sin\Theta_s^{(m)}(x)}{\ln\frac{T}{T_c}+\frac{2T}{T_c}\sum_0^{\tilde{\Omega}_{\max}}1/\tilde{\omega}} . \tag{A9}$$

Thus Eqs. (A8) and (A9) express $\tilde{\Delta}^{(m+1)}$ and $\tilde{\Delta}_s^{(m+1)}(x)$ through $\Theta^{(m)}$, $\Theta_s^{(m+1)}$, and $\tilde{\Delta}^{(m)}$ on the mth iteration step.

Solutions for Θ_s

To solve Eqs. (A1) and (A3) for Θ_s we use the linearization procedure

$$\Theta_s=\Theta_{s0}+\tilde{\Theta}_s , \tag{A10}$$

where $\tilde{\Theta}_s$ is a small correction on Θ_{s0}, i.e., for each iteration we calculate

$$\Theta_s^{(m+1)}=\Theta_s^{(m)}+\tilde{\Theta}_s . \tag{A11}$$

Equations (A1) and (A3) should now be solved for the function $\tilde{\Theta}_s(x)$. Expanding $\cos\Theta_s$ and $\sin\Theta_s$ we obtain for (A1) and (A3), respectively, the equations

$$\tilde{\Theta}_s''+g_0(x)\tilde{\Theta}_s=-f_0(x) , \tag{A12a}$$

$$\tilde{\Theta}_s'(0)+x_0\tilde{\Theta}_s(0)=-\varphi_0 , \tag{A12b}$$

where

$$g_0=-\tilde{\omega}\cos\Theta_{s0}-\tilde{\Delta}_s\sin\Theta_{s0} , \tag{A13a}$$

$$f_0=\Theta_{s0}''+\tilde{\Delta}_s\cos\Theta_{s0}-\tilde{\omega}\sin\Theta_{s0} . \tag{A13b}$$

At the boundary $x=0$ the constants x_0 and φ_0 are given by

$$x_0=-\gamma_m p\{\tilde{\omega}\cos\Theta_{s0}+\tilde{\Delta}_s\sin\Theta_{s0}-\gamma_B^2 p[\tilde{\omega}\sin\Theta_{s0}-\tilde{\Delta}\cos\Theta_{s0}]^2\} , \tag{A14a}$$

$$\varphi_0=\Theta_{s0}'-\gamma_m p(\tilde{\omega}\sin\Theta_{s0}-\tilde{\Delta}\cos\Theta_{s0}) , \tag{A14b}$$

where

$$p=[1+\gamma_B^2(\tilde{\omega}^2+\tilde{\Delta}^2)+2\gamma_B(\tilde{\omega}\cos\Theta_{s0}+\tilde{\Delta}\sin\Theta_{s0})]^{-1/2} . \tag{A14c}$$

The scheme Eqs. (A12)–(A14) is solved by the standard method of "forward elimination, backward substitution"; see, for example, Ref. 40.

*On leave from the Institute of Solid State Physics, 142432 Chernogolovka, Moscow District, Russia.

†Present address: University of Oxford, Department of Physics, Keble Road, Oxford OX1 3RH, United Kingdom.

[1] M. Gurvitch, M. A. Washington, and H. A. Huggins, Appl. Phys. Lett. **42**, 472 (1983).

[2] A. Shoji, M. Aoyagi, S. Koraka, F. Shinoki, and M. Hayakawa, Appl. Phys. Lett. **46**, 1098 (1985).

[3]N. R. Werthamer, Phys. Rev. **147**, 255 (1966).
[4]A. I. Larkin and Yu. N. Ovchinnikov, Sov. Phys. JETP **51**, 1535 (1966).
[5]For example, M. Gurvitch and J. Kwo, Adv. Cryog. Eng. **30**, 509 (1984).
[6]S. Morohashi, T. Imamura, and S. Hasuo, Appl. Phys. Lett. **60**, 3039 (1992).
[7]T. Shiota, T. Imamura, and S. Hasuo, Appl. Phys. Lett. **61**, 1228 (1992).
[8]J. Talvacchio, J. G. Gavaler, A. I. Braginski, and M. A. Janocko, J. Appl. Phys. **58**, 4638 (1985).
[9]T. M. Klapwijk (private communication).
[10]B. Wessely *et al.*, J. Appl. Phys. **72**, 584 (1992).
[11]N. Booth, Appl. Phys. Lett. **50**, 293 (1987).
[12]W. L. McMillan, Phys. Rev. **175**, 537 (1968).
[13]V. Z. Kresin, Phys. Rev. B **28**, 1294 (1983).
[14]G. B. Arnold, Phys. Rev. B **18**, 1076 (1978).
[15]E. L. Wolf and G. B. Arnold, Phys. Rep. **91**(2), 31 (1982).
[16]A. D. Zaikin and G. F. Zharkov, Zh. Eksp. Teor. Fiz. **78**, 721 (1980) [Sov. Phys. JETP **51**, 364 (1980)]; **81**, 1781 (1981) [**54**, 944 (1981)].
[17]G. Kieselmann, Phys. Rev. B **35**, 6762 (1987).
[18]M. Ashida, S. Aoyama, J. Hara, and K. Nagai, Phys. Rev. B **40**, 8673 (1989).
[19]Y. Tanaka and M. Tsukada, Phys. Rev. B **47**, 2754 (1993).
[20]U. Schlussler and K. Rummel, Phys. Rev. B **47**, 2754 (1993).
[21]A. A. Golubov and M. Yu. Kupriyanov, J. Low Temp. Phys. **70**, 83 (1988).
[22]A. A. Golubov and M. Yu. Kupriyanov, Sov. Phys. JETP **69**, 805 (1989).
[23]A. A. Golubov, M. A. Gurvitch, M. Yu. Kupriyanov, and S. V. Polonskii, Sov. Phys. JETP **76**, 915 (1993).
[24]G. Eilenberger, Z. Phys. B **214**, 195 (1968).
[25]K. Usadel, Phys. Rev. Lett. **25**, 560 (1970).
[26]M. Yu. Kupriyanov and V. F. Lukichev, Sov. J. Low Temp. Phys. **8**, 1045 (1982).
[27]M. Yu. Kupriyanov and V. F. Lukichev, Sov. Phys. JETP **67**, 1163 (1988).
[28]A. A. Golubov, in *Proceedings SPIE—Conference 215* (SPIE, Bellingham, WA, 1994), p. 353.
[29]K. Maki, in *Superconductivity,* edited by R. D. Parks (Marcel Dekker, New York, 1969), p. 1035.
[30]V. Ambegaokar and A. Baratoff, Phys. Rev. Lett. **10**, 486 (1969).
[31]H. Kroger, G. N. Smith, and D. W. Jillie, Appl. Phys. Lett. **39**, 280 (1981).
[32]M. Gurvitch, M. A. Washington, H. A. Huggins, and J. M. Rowell, IEEE Trans. Magn. **MAG-19**, 791 (1983).
[33]J. G. Gijsbertsen, H. Netel, E. P. Houwman, T. Kachliki, J. Flokstra, and H. Rogalla (unpublished).
[34]C. Kittel, *Introduction to Solid State Physics,* 5th ed. (Wiley, New York, 1976), p. 376.
[35]S. B. Kaplan, C. C. Chi, D. N. Langenberg, J. J. Chang, S. Jafarey, and D. J. Scalapino, Phys. Rev. B **14**, 4854 (1976).
[36]V. M. Krasnov, V. A. Oboznov, and V. V. Ryazanov, Physica C **196**, 335 (1992).
[37]R. Meservey and B. B. Schwartz, in *Superconductivity* (Ref. 29), p. 141.
[38]E. P. Houwman, D. Veldhuis, J. Flokstra, and H. Rogalla, J. Appl. Phys. **67**, 1992 (1990).
[39]B. A. Aminov (private communication).
[40]For example, E. L. Wachspress, in *Mathematische Methoden für Digitalrechner I,* edited by A. Ralston and H. S. Wilf (Oldenbourg Verlag, München, 1972), p. 217.